



HAL
open science

New constraints for dust models from Planck total and polarized emission

V. Guillet

► **To cite this version:**

V. Guillet. New constraints for dust models from Planck total and polarized emission. Galactic Astrophysics [astro-ph.GA]. Université Paris-Sud Orsay, 2015. tel-02022595

HAL Id: tel-02022595

<https://hal.science/tel-02022595>

Submitted on 18 Feb 2019

HAL is a multi-disciplinary open access archive for the deposit and dissemination of scientific research documents, whether they are published or not. The documents may come from teaching and research institutions in France or abroad, or from public or private research centers.

L'archive ouverte pluridisciplinaire **HAL**, est destinée au dépôt et à la diffusion de documents scientifiques de niveau recherche, publiés ou non, émanant des établissements d'enseignement et de recherche français ou étrangers, des laboratoires publics ou privés.

New constraints for dust models from *Planck* total and polarized emission

Habilitation à Diriger des Recherches

présentée et soutenue publiquement le mercredi 16 décembre 2015

par

Vincent Guillet

Composition du jury

Rapporteurs : Ralf Siebenmorgen (ESO, Garching)
Martin Giard (IRAP, Toulouse)
Pierre Hily-Blant (IPAG, Grenoble)

Examineurs : Karine Demyk (IRAP, Toulouse)
Jérôme Pety (IRAM, Grenoble)
Guillaume Pineau des Forêts (IAS, Orsay)

Pour me contacter : vincent.guillet@ias.u-psud.fr

Mis en page avec la classe thloria.

Table des matières

Foreword	3
1 A need for dust evolution in the diffuse ISM	5
1.1 Introduction to dust evolution	5
1.2 Correlation of <i>Planck</i> data with HI maps.	6
1.3 Correlation of <i>Planck</i> data with extinction measurements	7
1.4 Dust models confronted to <i>Planck</i> observations	8
2 Introduction to dust polarization	11
2.1 Basic physics of dust polarization	12
2.1.1 Starlight polarized by dust extinction	12
2.1.2 Dust polarized thermal emission	13
2.2 Grain dynamics	14
2.2.1 Spinning	15
2.2.2 Precession around magnetic field lines	15
2.3 Grain alignment along the magnetic field lines	15
2.3.1 Generalities on dust alignment	16
2.3.2 Magnetic alignment : the magnetic relaxation	17
2.3.3 Radiative alignment : the radiative torques (RATs)	18
2.3.4 Mechanical alignment : alignment in gas flows	21
2.3.5 Other subtleties in the grain alignment dynamics	21
2.4 Observational constraints from dust polarization	22
2.4.1 Spectral information	22
2.4.2 Observational constraints on dust alignment	24
2.5 Dust models satisfying these pre- <i>Planck</i> constraints	25

3	Statistical properties of dust polarized emission as seen by <i>Planck</i>	27
3.1	Manipulating full-sky polarization data	27
3.2	Statistical properties of dust polarized emission from the <i>Planck</i> HFI 353 GHz channel	29
3.2.1	Anticorrelation between the polarization fraction P/I and the apparent magnetic field disorder	31
3.2.2	Decrease of P/I with increasing column density	33
3.2.3	Does <i>Planck</i> brings new constraints on dust alignment?	33
4	Coupling between the gas and the magnetic field	35
4.1	Relative orientation of the magnetic field with the gas structures	35
4.2	Structure of the magnetic field in dense structures	36
5	Dust models and <i>Planck</i> results in polarization	39
5.1	Spectral properties of dust in polarization as seen by <i>Planck</i>	39
5.2	Maximal dust polarization fraction in extinction and in emission	41
5.3	Synthetic view on <i>Planck</i> observational constraints for dust models	43
5.4	Toward new dust models (<i>work in progress</i>)	44
5.4.1	Constraints on the optical properties of the aligned population	46
5.4.2	Models for the low-latitude diffuse ISM	47
5.4.3	Conclusion	51
6	Conclusion & Perspectives	52
6.1	Dust evolution and polarization	52
6.2	Future works (short term)	53
6.3	Mid-term perspectives	54
7	Appendix	55
	Bibliographie	58

Forword

Dust is the solid phase of the interstellar medium, a minor constituent (less than 1% of the gas mass) spanning a large range of sizes from a fraction of a nanometer to a fraction of a micrometer. It is responsible for the reddening (Trumpler 1930) and polarization (Hall 1949) of starlight. Dust is observed both in polarized and total extinction (*e.g.* Mathewson & Ford 1971; Fitzpatrick & Massa 1990) and through its thermal (Perault et al. 1987; Hildebrand et al. 1999) and non-thermal (Kogut et al. 1996) emission.

Dust emission is routinely used to trace the star formation activity in outer galaxies and infer their gas content (*e.g.* Pannella et al. 2015). Dust emission is optically thin in the submillimeter, and unlike atomic and molecular emission, gives access to the full gas content in all phases, ionized, atomic and molecular, even in the H₂-dominated regions not traced by the HI 21-cm and CO emission, the so-called "Dark Gas" (Planck Collaboration XX 2011). Still, variations in the optical properties of dust accross and within phases ("Dust Evolution", see *e.g.* Flagey et al. 2009; Köhler et al. 2015), as well as instrinsic variations in the Gas-to-Dust ratio (*e.g.* Roman-Duval et al. 2014), can complicate the derivation of the gas mass from dust emission.

Dust is also used to trace the interstellar magnetic field through its polarized imprint on starlight (*e.g.* Frisch et al. 2012; Berdyugin et al. 2014; Franco & Alves 2015) as well as through its own polarized thermal emission (Zeng et al. 2013; Planck Collaboration Int. XIX 2015; Fissel et al. 2015). Unlike synchrotron polarization, dust polarization traces the magnetic field correlated with interstellar matter, from the most diffuse medium down to the formation of stars.

Dust is also in itself a source of interest. In this paper, I will present my contributions to a better understanding of dust nature and optical properties. Most of this work has been done within the *Planck* collaboration, and within the pleasant and happy atmosphere of the MISTIC ERC team lead by F. Boulanger. It is the result of a *collective* work, with a lot of interactions within our group, especially on the subject of polarization for which we all had everything to learn.

Thanks to the *Planck* multiwavelength coverage, there has been considerable work toward a better understanding of the observed variations of the dust Spectral Energy Distribution (SED) through the diffuse ISM, which I summarize in Chapter 1. Because the polarization capacities of *Planck* are the most original part of this mission, this paper will then focus on dust polarization for which I wrote a brief introduction (Chapter 2). The analysis and understanding of the statistical properties of dust polarized emission measured by the *Planck* HFI instrument took us a while, and is presented in Chapter 3, with a brief mention of my contribution to the understanding of the structure of the magnetic field in the diffuse and

dense ISM (Chapter 4). I conclude with a chapter dedicated to a work in progress in our group on the revision of dust models to satisfy *Planck* constraints (Chapter 5).

I wish to thank the whole MIS team of the IAS for the helpful and pleasant working conditions that also makes this job enjoyable. I also thank the jury for kindly accepting my invitation.

Chapitre 1

A need for dust evolution in the diffuse ISM

This first chapter deals with the recent constraints brought by *Planck* on the variations of the dust properties in the diffuse ISM.

1.1 Introduction to dust evolution

Dust properties are not fixed through the ISM. Variations in the wavelength-dependence of the dust extinction curves have been known for long (Fitzpatrick & Massa 1988; Cardelli et al. 1989), with many "anomalous curves" (e.g. Mazzei & Barbaro 2008). The variance is so large that it is even hard to maintain the idea of an "average" extinction curve in the ISM : each line of sight merely reflects the response of dust to local conditions, unique to each line of sight (Fitzpatrick & Massa 2007).

Such variations were also observed in various FIR and submillimeter experiments in the transition from the diffuse to the dense ISM (Stepnik et al. 2003; Del Burgo & Laureijs 2005; Ridderstad et al. 2006; Martin et al. 2012; Planck Collaboration XXV 2011; Ysard et al. 2013). Could these variations be accomodated by changing the free parameters of dust models, namely the size distributions of grains and the radiation field intensity ? The answer is no. All these studies concluded that, in order to explain those variations, the intrinsic optical properties of dust had to change from the outer to the inner parts of clouds, and not only the size distributions or the grain heating by starlight. We name *dust evolution* the fact that dust models can not explain the observed variations of SEDs *with fixed optical properties for dust grains*. Among others, we have demonstrated that the onset of coagulation is a plausible process to explain those variations observed when entering molecular clouds (Köhler et al. 2011).

As I will present below, *Planck* observations confirm that dust evolves even in the most diffuse, high latitude, ISM. In such a low density gas, coagulation is however not likely to occur because it is too slow. Other processes will have to be considered (e.g. Jones et al. 2013).

The *Planck* HFI observations have now opened a new era for the modeling of dust emission, an era of high precision. Its frequency coverage with 6 channels from 857 down

to 100 GHz allowed for a precise measurement of the dust temperature and spectral index β ; the unprecedented precision of its calibration (better than 1% at the lowest frequencies of HFI) is now a challenge for dust models; the wealth of the full-sky statistics (more than 50,000,000 pixels at full resolution) provides a complete description of the variations of dust emission through the ISM.

In this chapter, I present some aspects of the work I have been involved in, within the MISTIC team of the *Planck* collaboration, on the study of the variations of the dust SED in total intensity. In Section 1.2, I present the results of the correlation of dust maps with HI 21-cm maps. In Section 1.3, I show which information we gain by correlating with another dust tracer, the dust extinction in the optical. I conclude in Section 1.4 with the presentation of the work by my student Lapo Fanciullo on the confrontation of those results with three physical dust models.

1.2 Correlation of *Planck* data with HI maps.

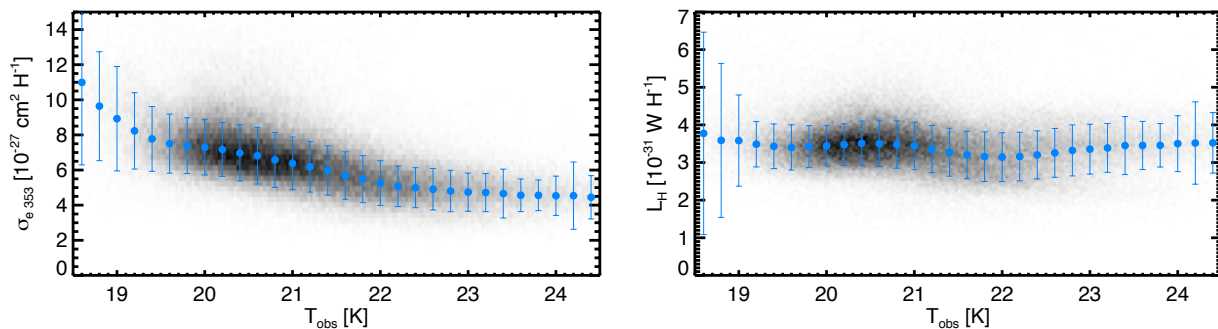


FIGURE 1.1 – Dust opacity (left) at 353 GHz $\sigma_e = \tau_{\nu_0}/N_H$ and dust specific luminosity (right) $L_H = 4\pi\mathcal{R}/N_H$ as a function of the observed dust temperature. From [Planck Collaboration XI \(2014\)](#).

[Planck Collaboration XI \(2014\)](#) characterized the variations of dust temperature, spectral index and emissivity in the high-latitude sky through a modified blackbody fit

$$I_\nu = \tau_{\nu_0} B_\nu(T_{\text{obs}}) \left(\frac{\nu}{\nu_0} \right)^{\beta_{\text{obs}}} \quad (1.1)$$

where $\nu_0 = 353$ GHz is the reference frequency, T_{obs} the observed dust temperature, and β_{obs} the observed dust spectral index. With the version of the data used at the time of publication (DX9), the dust SED was well fitted by such a model, though with some indication of a mild flattening of the SED in the submillimeter ([Planck Collaboration Int. XVII 2014](#)). This flattening has now disappeared from the latest version of the data (DX11d), which is improved in terms of systematics.

This article introduced, after [Martin et al. \(2012\)](#), an interesting quantity, the *radiance* \mathcal{R} . The radiance is the total power emitted by dust :

$$\mathcal{R} = \int_\nu I_\nu d\nu = \tau_{\nu_0} \frac{\sigma_S}{\pi} T_{\text{obs}}^4 \left(\frac{k T_{\text{obs}}}{h\nu_0} \right)^{\beta_{\text{obs}}} \frac{\Gamma(4 + \beta_{\text{obs}}) \zeta(4 + \beta_{\text{obs}})}{\Gamma(4) \zeta(4)} \quad (1.2)$$

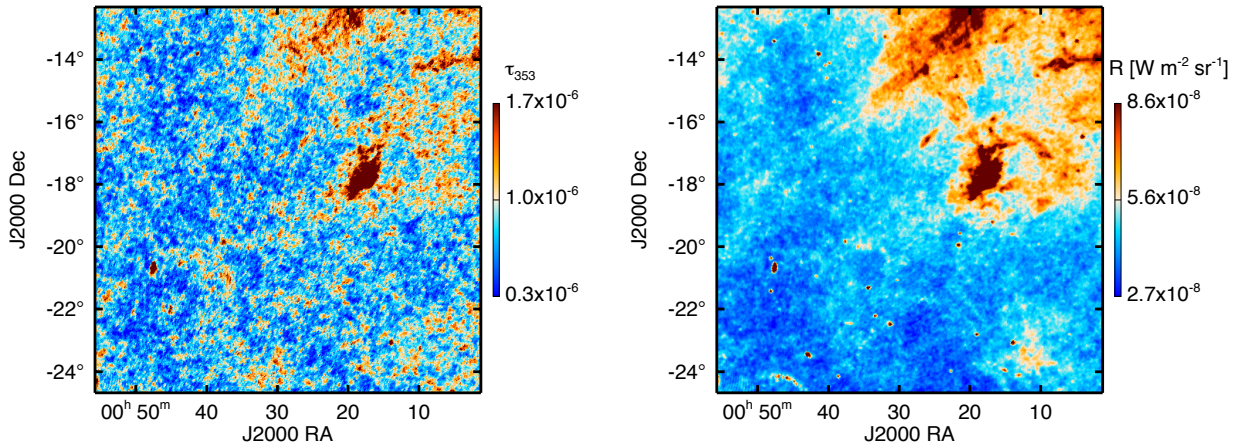


FIGURE 1.2 – Map of τ_{353} (left) and \mathcal{R} (right) of a diffuse area of the sky, centred on $l = 90^\circ$, $b = -80^\circ$. From [Planck Collaboration XI \(2014\)](#).

where σ_S is the Stefan-Boltzmann constant, k is the Boltzmann constant, h is the Planck constant. By conservation of the energy, \mathcal{R} is equal to the total power absorbed by the same large dust grains responsible for the FIR dust emission. The radiance therefore only depends on the dust absorption properties from the UV to the NIR, and on the intensity of the radiation field G_0 . As a consequence, *the radiance has the nice property of being independent of the dust optical properties in emission.*

We found that the dust emissivity per proton, $\sigma_e = \tau_{\nu_0}/N_H$, was anticorrelated with the observed dust temperature, T_{obs} , while the dust radiance per proton, L_H , showed no such dependence (Fig. 1.1). This was interpreted as an indication of the variation of the dust FIR emissivity in this very diffuse ISM : variations of the dust temperature could not be attributed only to variations in the heating of dust (*i.e.* of the radiation field intensity), but also to intrinsic variations of the dust optical properties. Such a variation of dust emissivity limits our precision in the conversion of the dust optical depth to a gas column density. In such tenuous medium, coagulation of dust grains could not reasonably be invoked so that an alternative had to be looked for.

The radiance map turned out, surprisingly to us, to be less clumpy than the optical depth : the integral in \mathcal{R} removes most of the contamination by the Cosmic Infrared Background which is decorrelated between frequencies, thus providing nice maps of the most diffuse ISM as can be seen in Fig. 1.2. Because the radiance map is less clumpy than the map of optical depth, and independent of emissivity variations, the radiance map was preferred over the optical depth to provide an extinction $E(B - V)$ map at very low column densities.

1.3 Correlation of *Planck* data with extinction measurements

The correlation of dust emission with HI data has a few limitations : 1) one is restricted to very low column densities to guarantee that the column density of H_2 can be safely ignored ; 2) the results of the correlation analysis, τ_{ν_0}/N_H , integrates an unknown parameter, the dust-to-

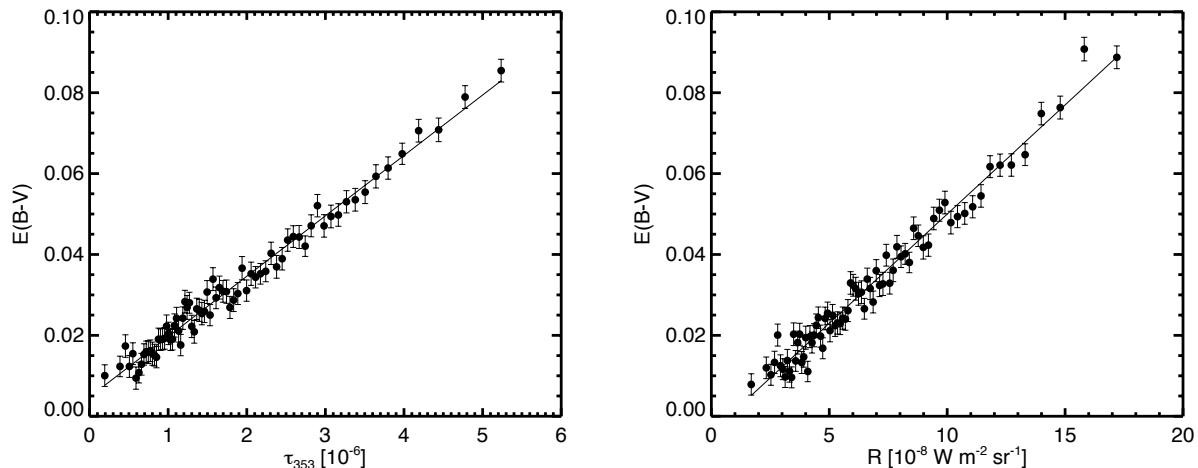


FIGURE 1.3 – $E(B - V)$ measured with quasars in the diffuse ISM at high Galactic latitude as a function of τ_{353} (left) and \mathcal{R} (right). Each point is the average of $E(B - V)$ values in a bin of τ_{353} or \mathcal{R} . From [Planck Collaboration XI \(2014\)](#).

gas ratio, which for dust modeling complicates the interpretation of $\tau_{\nu_0}/N_{\text{H}}$ in terms of dust evolution; 3) what really matters for people studying outers galaxies is the dust reddening correction $E(B - V)$ to apply to their data. Finding a recipe to convert *Planck* observations to a reddening, an update of [Schlegel et al. \(1998\)](#), would be useful.

To get this pure dust-to-dust observable constraint, one can correlate dust emission with dust extinction. This was done with the modified blackbody approach described in the previous section. Using $\sim 200,000$ extinction measurements towards Quasars from the Sloan Digital Sky Survey ([Schneider et al. 2010](#)), [Planck Collaboration XI \(2014\)](#) found a strong correlation between τ_{ν_0} or \mathcal{R} and the $E(B - V)$ from quasars (Fig. 1.3). A similar conclusion was drawn in molecular regions by correlating τ_{ν_0} and \mathcal{R} with the total extinction A_{V} obtained from near-infrared color excess of the 2MASS database ([Schneider et al. 2011](#)). In the denser environments probed by stars, the optical depth τ_0 appeared to be a better tracer of column density than \mathcal{R} , especially in those molecular regions where the radiation field intensity (which drives \mathcal{R}) varies significantly, like around ρ Ophiuchi.

1.4 Dust models confronted to *Planck* observations

A similar work was done in [Planck Collaboration Int. XXIX \(2014\)](#), using a physical dust model rather than a blackbody fit. The dust SED (a combination of WISE, IRAS, DIRBE and *Planck* data) over the whole sky was fitted with the [Draine & Li \(2007\)](#) dust model. The model fitted the data very well. From the fitting, we were able to derive an extinction map $A_{\text{V}}^{\text{DL07}}$, as well as a map of the radiation field U_{min} . Restricting the results to the lines of sight to QSOs from the SDSS catalog (see previous section), we correlated $A_{\text{V}}^{\text{DL07}}$ with the observed dust extinction to the quasars, $A_{\text{V}}^{\text{QSO}}$, binning the lines of sight in 20 bins in U_{min} . The fitted parameter $A_{\text{V}}^{\text{DL07}}$ was found to be systematically overestimated with respect to $A_{\text{V}}^{\text{QSO}}$ (Fig. 1.4, left). The error factor $A_{\text{V}}^{\text{DL07}}/A_{\text{V}}^{\text{QSO}}$ depends on the fitted parameter U_{min} , and

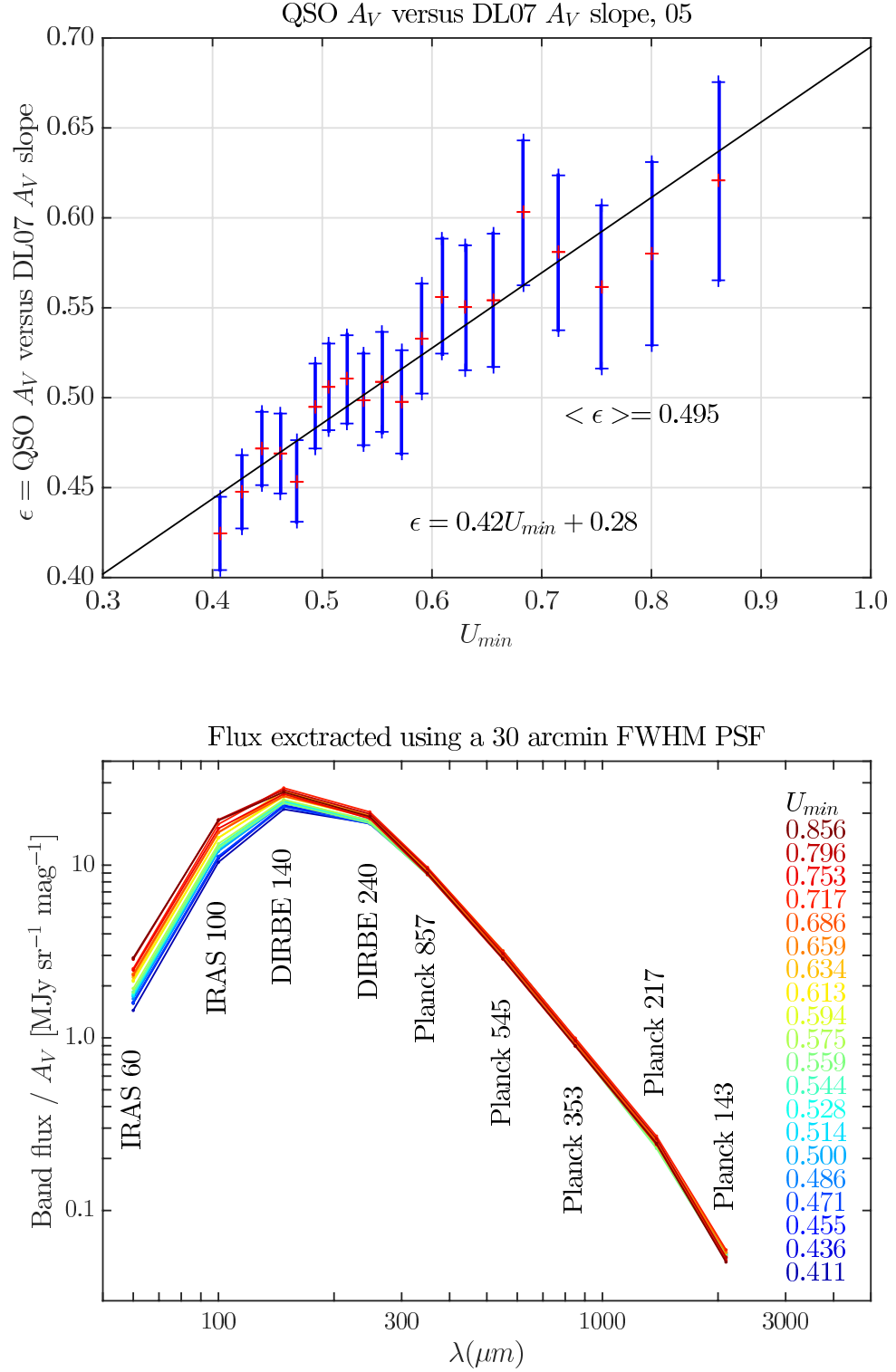


FIGURE 1.4 – (Top) Ratio of the observed A_V toward QSOs to the fitted A_V from the [Draine & Li \(2007\)](#) model, as a function of the fitted dust temperature (U_{\min} parameter). (Bottom) the 20 SEDs derived from the correlation of the dust SED binned in temperature (U_{\min} parameter) with extinction measurements to QSOs from SDSS. From [Planck Collaboration Int. XXIX \(2014\)](#).

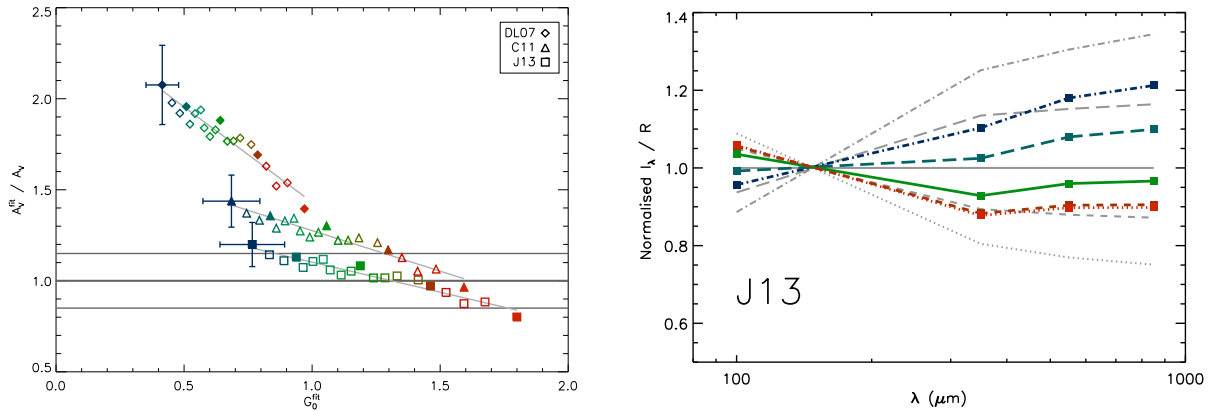


FIGURE 1.5 – (Left) Ratio between the fitted and observed A_V for the 20 SEDs of [Planck Collaboration Int. XXIX \(2014\)](#), with three dust models ([Draine & Li 2007](#); [Compiegne et al. 2011](#); [Jones et al. 2013](#)). (Right) Predictions for the dust SED with the [Jones et al. \(2013\)](#) model. Each model is normalized by its radiance. To emphasize the differences, all SEDs are divided by the center SED of the [Planck Collaboration Int. XXIX \(2014\)](#) sample. From [Fanciullo et al. \(2015\)](#)

has a mean value of ~ 2 . From this error factor we infer that : 1) the dust optical properties used in [Draine & Li \(2007\)](#) (astrosilicates and graphite) are not emissive enough ; 2) the dust emissivity per unit extinction varies through the diffuse ISM.

The A_V -normalized SEDs were averaged in each U_{\min} bin, thus providing 20 SEDs ordered by their temperature¹ (Fig. 1.4, right). These SEDs per unit extinction are representative of the variations in the SEDs observed in the whole diffuse ISM. They look very similar in the *Planck* bands, but differ at the shorter wavelengths.

We further tested two others models in the work by my PhD student Lapo Fanciullo ([Fanciullo et al. 2015](#)) : the [Compiegne et al. \(2011\)](#) and [Jones et al. \(2013\)](#) dust models. In this fitting, the size distributions were fixed, and only the radiation field intensity was allowed to vary. [Jones et al. \(2013\)](#) was found to be the model closest to the data, while [Compiegne et al. \(2011\)](#) systematically overestimated the extinction A_V by $\sim 25\%$ (Fig. 1.5, left). All models failed to explain the observed variations of the SED by playing on the radiation field intensity, thus demonstrating that the need for dust evolution is model-independent.

From the fit to the SED with a physical model, one derives the extinction in the optical A_V and the radiation field G_0 . If A_V is biased (overestimated), then G_0 is also biased (underestimated).

1. The U_{\min} parameter is primarily constrained by the wavelength of the peak of the SED, and is thus a measurement of dust temperature.

Chapitre 2

Introduction to dust polarization

Starlight polarization was first observed more than 60 years ago ([Hall 1949](#); [Hiltner 1949](#)). The measured direction of polarization for neighbouring stars being similar, it was inferred that this polarization is not intrinsic to the stars, but must be of interstellar origin. A weak correlation between the degree of starlight polarization and the reddening to the star gave an indication of what is now confirmed through many observations : interstellar dust grains, which are responsible for the reddening of starlight, are also responsible for its polarization.

From the polarization of starlight by interstellar dust, we infer that

1. dust grains are elongated (which is not unexpected) ;
2. the grain spin axis keeps a preferred direction when averaged over the grain dynamics, which we call the direction of alignment ;
3. the direction of alignment of dust grains is consistent on large (parsec-like) scales.

The reason for the large-scale order of the dust alignment direction was initially debated : were dust grains aligned along the magnetic field lines ([Spitzer & Tukey 1949](#); [Davis & Greenstein 1949](#)) or along the streaming lines of gas flows ([Gold 1952](#))? The magnetic interpretation was reinforced by the later mapping of the polarization of more than 1,800 stars by [Mathewson & Ford \(1971\)](#), which revealed that the direction of polarization traced the spiral arms as well as HII bubbles. *Dust polarization therefore traces the magnetic field.*

Polarization observations have recently accelerated their development, with huge data sets becoming available to the community. Some are motivated by the mapping of the magnetic field in star-forming regions, whether from the ground (SCUPOL, [Poidevin et al. 2013](#)) or with balloons (BLASTPol, [Fissel et al. 2015](#)). Some others by the characterization of the various polarized foregrounds to the CMB polarization : the *Planck* satellite ([Planck Collaboration Int. XIX 2015](#)) with its channels operating from 353 GHz down to 30 GHz, the ground experiment QUIJOTE operating in the frequency range 10-42 GHz ([Génova-Santos et al. 2015](#)), and the recently launched PILOT balloon operating at 1.2 THz (240 μm) ([Misawa et al. 2014](#)). Polarization observations in extinction are now also becoming large surveys, with the measurement of polarization towards millions of stars in the Galactic Plane (GPIPS, [Clemens et al. 2012](#)), and a future mapping of the southern hemisphere (SOUTH POL, [Magalhaes 2014](#)).

2.1 Basic physics of dust polarization

Starlight polarization reveals the linear dichroism of the ISM, an asymmetry in the interstellar dust extinction or emission for two perpendicular directions of the oscillating electric field.

2.1.1 Starlight polarized by dust extinction

Individually, aspherical grains tend to scatter² and absorb starlight more efficiently if the incoming electric field is parallel to their largest axis, than to their shortest axis. This asymmetric extinction results in the polarization of an incoming unpolarized light, with a direction of polarization parallel to the short axis of the grain, which is also its spin axis.

The capacity of one single grain to polarize the transmitted light will depend on multiple factors : the grain shape, size and composition (its optical constant at the wavelength of observation), the orientation of the magnetic field with respect to the line of sight, and the efficiency of the grain alignment along the magnetic field (which depends on the local physical conditions as well as on the grain properties : namely shape, magnetic and optical properties).

When dust grains are aligned along a common direction on large scales (that of the magnetic field), the polarization pattern imprinted on starlight by all grains taken together do not cancel each other and result, by integration on the line sight, in a net polarization of starlight. From the measure of starlight polarization, we obtain two observables :

The polarization or position angle ψ The direction of starlight polarization is that of the magnetic field projected onto the plane of the sky. This direction must be considered as an averaged quantity, integrated on the line of sight, and ponderated by the local polarization capacity of dust.

The polarization degree p By definition,

$$p = \frac{F_{\parallel} - F_{\perp}}{F_{\parallel} + F_{\perp}} = \frac{\exp^{-\tau_{\parallel}} - \exp^{-\tau_{\perp}}}{\exp^{-\tau_{\parallel}} + \exp^{-\tau_{\perp}}} = \tanh \frac{\tau_{\parallel} - \tau_{\perp}}{2} \quad (2.1)$$

where F_{\parallel} and F_{\perp} are the fluxes along the 2 orthogonal polarization directions yielding respectively the highest and lowest fluxes, and τ_{\parallel} and τ_{\perp} the corresponding dust optical depths (Draine & Fraisse 2009). For weak extinction, this can be linearized into :

$$p \simeq \frac{\tau_{\parallel} - \tau_{\perp}}{2} \quad (2.2)$$

The observed starlight polarization degree p has the same dependence with dust properties, magnetic field orientation, and alignment efficiency as the isolated grain polarizing efficiency. Through the integration over the line of sight, p is furthermore, in the special case of a uniform medium, proportional to the dust total optical depth, τ . As usually in astrophysics,

2. Contrary to what is often written, dust polarization in extinction is not predominantly caused by absorption, but by scattering (Martin 2007).

the interpretation of p is complicated by possible variations of all factors on the line of sight. Still, one effect is unique to polarization. The superposition on the line of sight of screens of dust with comparable optical depths and directions of polarization perpendicular to each other will lead to a weak if not zero net polarization, even if each screen is individually strongly polarizing. This means that p , after its dependencies on dust properties, alignment efficiencies, and magnetic field orientation with respect to the line of sight, *also depends on the possible fluctuations of the plane-of-the-sky component of the magnetic field on the line of sight*. This high level of degeneracy make the interpretation of p quite difficult.

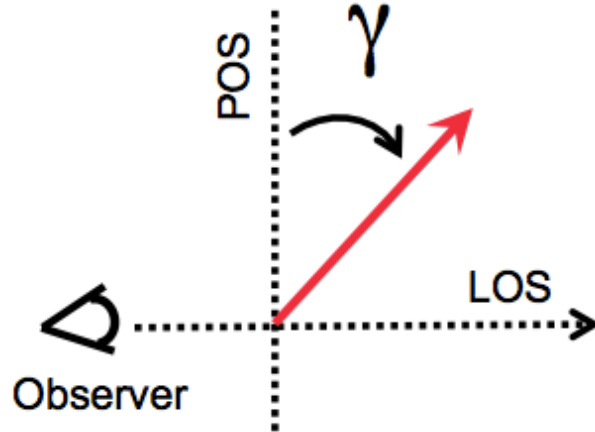
The polarization fraction p/τ From the measure of p and τ , one can derive another useful observable, the polarization fraction, p/τ (sometimes defined in the optical as p/A_V , with $A_V = 1.086 \tau_V$). Contrary to what is frequently written in the literature (*e.g.*, [Cashman & Clemens 2014](#)), p/τ is *not* a measure of the alignment efficiency of dust grains. The polarization fraction p/τ *also* entails the full complexity of the dependence of p with the structure of the magnetic field along the lines of sight, and with the grain shape and optical properties. Though the dependence of p on the column density has been removed in p/τ , one has introduced as a counterpart another complexity in the ratio : while p , for what is related to dust, depends on the optical properties of the population of aligned grains alone - and only large ($\geq 0.05 \mu\text{m}$) grains are aligned, see Section 2.4.1 - τ depends on the optical properties of grains of all compositions and sizes, whether aligned or not.

2.1.2 Dust polarized thermal emission

It was soon realized that if dust grains did polarize starlight by extinction, their thermal emission would also be polarized ([Stein 1966](#)). Aspherical grains behave like antennas and emit thermally in the far-infrared an electromagnetic wave that is partially polarized parallel to their largest axis. The direction of polarization in emission is therefore perpendicular to that in extinction, and to that of the local magnetic field.

The dust polarized emission, P (unit MJy/sr), is the analog of the starlight polarization degree p , and is therefore affected by the same dependencies (see Section 2.1.1). The fraction of polarization in emission, P/I , is the analog of p/τ .

The theory for dust polarized emission is much less complicated than for dust polarization by extinction. In the Rayleigh regime applicable to dust emission ($x = 2\pi a/\lambda \ll 1$ and $|m|x \ll 1$, with $m = n + ik$ the complex refractive index of the material), scattering is negligible and the electromagnetic oscillating field can be assumed to be uniform at one instant through the grain. Thanks to these simplifications, there exists analytical solutions to the expressions of the dust polarization cross-sections in the body frame ([Li et al. 2002](#)). In the Rayleigh limit, the response of the grain to an incoming electromagnetic wave (characterized by 2 oscillating fields, electric and magnetic, perpendicular to each other and to the direction of propagation of the wave) does not depend on the direction of the oscillating magnetic field, but only on that of the electric field (*e.g.*, [Draine & Fraisse 2009](#)). This allows for further simplifications for the expression of the polarization cross-section over the grain dynamics spinning and precessing around the magnetic field. The appendix (Chapter 7) recalls these expressions for homogeneous grains of oblate (pancake-like) and prolate (cigar-like) shape.

FIGURE 2.1 – From [Planck Collaboration Int. XXXIV \(2014\)](#).

The fractional polarization in emission has an analytical expression with the magnetic field geometry and dust alignment efficiency, in the simplified case of a uniform medium with homogeneous physical conditions :

$$\frac{P}{I} = p_{\max} R_{\text{rf}} F \cos^2 \gamma \quad (2.3)$$

- γ is the angle between the magnetic field and the plane of the sky (Fig. 2.1).
- R_{rf} is the Rayleigh reduction factor, which quantifies the level of dust alignment with the magnetic field lines. $R_{\text{rf}} = (3 \langle \cos^2 \beta \rangle - 1)/2$ where β is the angle between the spin axis of the grain and the direction of the magnetic field, and the average is done over the precession and spin dynamics of the grain (*e.g.*, [Roberge & Lazarian 1999](#)).
- F is a depolarization factor ($0 \leq F \leq 1$), intended to model the possible loss of polarization by turbulence (along the line of sight, within the beam) or by the superposition of layers of dust with different orientation for the plane-of-the-sky component of the magnetic field on the line of sight. This factor is related to the structure function S defined in Chapter 3, Section 3.2.1.
- p_{\max} is the dust *intrinsic* polarization fraction, the polarization fraction that would be observed if the magnetic field was uniform ($F = 1$), in the plane of the sky ($\gamma = 0$), and dust grains were perfectly aligned ($R_{\text{rf}} = 1$). The parameter p_{\max} only depends on the dust differential cross-sections, *i.e.* on the shape, size distribution and optical properties of dust grains.

2.2 Grain dynamics

Dust polarization in extinction and in emission would not be observed without the existence of a physical process aligning grains along the local magnetic field. In this section, I present a short review on the subject of grain alignment which I hope the reader will find useful.

The basic physics of dust alignment is that of spinning tops, precessing around magnetic field lines.

2.2.1 Spinning

Dust grains spin fast. They continuously exchange momentum with their environment. When a dust grain is struck by a gas particle, its angular momentum is increased or decreased. Assuming equipartition between the grain rotational energy and the gas thermal energy (with $T \sim 100$ K for the diffuse medium), a spherical grain with radius $a = 0.1 \mu\text{m}$ would rotate at a frequency ~ 100 MHz (Davis & Greenstein 1951). Grains could even rotate suprathermally, through non-thermal processes : the absorption and emission of photons affects the grain angular momentum, as well as the recoil from the ejection of H_2 molecules formed at its surface (Purcell 1979).

2.2.2 Precession around magnetic field lines

There are different ways how dust grains can acquire a magnetic moment which will make them precess around magnetic field lines. All materials show some magnetic response, or *magnetization* (also called magnetic polarization by analogy with the electric polarization).

- *Paramagnetic* materials (*e.g.* silicates) will magnetize in the presence of an external magnetic field \mathbf{B} . The magnetization \mathbf{M} is parallel to \mathbf{B} (their magnetic susceptibility χ is positive) and its intensity increases linearly with the intensity of the auxiliary field \mathbf{H} : $\mathbf{M} = \chi\mathbf{H}$ with $\mathbf{B} = \mathbf{H} + 4\pi\mathbf{M}$.
- Thanks to their unpaired electron spins, *ferromagnetic* materials (metallic iron, iron oxides such as magnetite Fe_3O_4) possess a permanent magnetization. Such materials could be found in the form of free-flying particles of a single ferromagnetic domains, or as inclusions in a paramagnetic matrix ("superparamagnetism") (Jones & Spitzer 1967; Draine & Hensley 2013). Ferromagnetic and superparamagnetic materials have a magnetic susceptibility orders of magnitude higher than paramagnetic materials.
- The *Barnett* effect : an uncharged paramagnetic or ferromagnetic body will spontaneously magnetize when spinning, *in the absence of any external magnetic field*, acquiring a magnetization $\mathbf{M} = \chi/\gamma\boldsymbol{\Omega}$ parallel to its spin axis, with $\boldsymbol{\Omega}$ the angular velocity vector of the grain, and γ the gyromagnetic ratio of the *electron* spins (Barnett 1915; Dolginov & Mitrofanov 1976; Purcell 1979; Weingartner & Draine 2003). By transferring angular momentum from the rotation to the spin system of the material, angular momentum can be conserved while decreasing the rotational energy.
- The *Rowland* effect : a charged spinning grain will also acquire a magnetic moment through the current created by the circulation of its electron (Martin 1971). This effect is however small (Davis & Greenstein 1951).

2.3 Grain alignment along the magnetic field lines

After a brief presentation on some generalities about grain alignment and disalignment processes, I will present three alignment theories : alignment by magnetic dissipation, by

radiative torques, and by gas flows.

2.3.1 Generalities on dust alignment

Our magnetized grains are now spinning and precessing around magnetic field lines. Still, these grains are not able to significantly polarize starlight because they are not *sufficiently well* aligned. Grain alignment will proceed in two steps, first aligning the main axis of inertia, \hat{a} , with its angular momentum \mathbf{J} , and then \mathbf{J} with \mathbf{B} :

Internal alignment of \mathbf{J} and \hat{a} Rigid bodies do not spontaneously rotate around their axis of maximal inertia, \hat{a} . The first step toward alignment will be the alignment of the grain rotational velocity Ω (or angular momentum \mathbf{J}) with its axis of maximal inertia, \hat{a} . For this, the grain must dissipate *internally* some of its rotational energy while still conserving its angular momentum. This can happen through the Barnett effect (see Section 2.2.2). If the grain is not rotating around \hat{a} , then Ω , and subsequently the magnetization \mathbf{M} induced by the Barnett effect, precesses continuously in the frame of the grain. The continuous change of the direction of magnetization through the material dissipates energy, toward a minimum that is reached when the grain rotates around \hat{a} and the magnetization \mathbf{M} , parallel to \hat{a} , conserves a fixed direction in the grain coordinates (Purcell 1979). This internal relaxation, which corresponds to the alignment of Ω , \mathbf{J} and \hat{a} , is a fast process : $\tau \sim 10^{-5}$ s (Purcell 1979; Lazarian & Draine 1999; Lazarian 2007)

Lazarian & Draine (1999) demonstrated that the spins of *protons*, like the spins of electrons in the Barnett effect, could also produce a dissipation when the grain does not rotate around its axis of maximal inertia. They named it *nuclear relaxation*. They showed that the nuclear relaxation can be orders of magnitude more important than the Barnett relaxation for slowly rotating grains, thus insuring the alignment of \mathbf{J} with \hat{a} even at low rotational velocities.

Torques aligning the grain spin axis with \mathbf{B} Grain is now spinning around its axis of maximal inertia \hat{a} with a momentum \mathbf{J} , and is precessing around \mathbf{B} , thus providing a *mean* alignment of the spin axis with \mathbf{B} . Alignment of \mathbf{J} with \mathbf{B} is however at this stage not sufficient to significantly polarize starlight. A physical process is needed to align the grain angular momentum better or even perfectly with \mathbf{B} . The situation is in fact similar to that of a top spinning on a table (Davis & Greenstein 1951). Just like the magnetic field, the gravitational field provides the torque responsible for the precession of the spin axis of the top around the vertical axis. When the top is launched, it is precessing at large angles with respect to the vertical. It is not gravity but the small frictional torque exerted at the pivot that will damp the wobbling and nutation of the grain, as well as slowly rise the spin axis toward a partial or even perfect alignment with the vertical. This analogy supports the important conclusion that the torque aligning the spin axis of dust grains along the magnetic field *does not have to be of magnetic origin* : the currently most popular model of grain alignment (radiative torques) indeed relies on torques exerted by the *stellar radiation field*.

Disalignment torques When the grain collides with a gas particle, or emits an infrared photon, the exchange of momentum results in a random torque which tends to disalign the grain. For large grains ($a > 0.1 \mu\text{m}$), the dominant drag is through collisions with the gas, while for small grains ($a \sim 0.1 \mu\text{m}$) it is infrared emission (Draine & Lazarian 1998).

Supra-thermal rotation Supra-thermal rotation is a key ingredient for dust alignment. Through the gyroscopic effect, supra-thermal rotation provides a stability to the spinning of the grain against random disaligning torques. It can be driven by H_2 torques (pinwheel torques, Purcell 1979) or by radiative torques (Draine & Weingartner 1996; Lazarian & Hoang 2007).

2.3.2 Magnetic alignment : the magnetic relaxation

The alignment of dust grains considered as permanent magnets, among the first ideas to have appeared after the discovery of starlight polarization, can be excluded. The torque needed to counterbalance the gyroscopic torque would necessitate a magnetic field intensity which is far too high for the diffuse ISM ($B \sim 10^{-4}$ Gauss, Spitzer & Tukey 1949; Davis & Greenstein 1951), even in the optimistic case of a grain with a single ferromagnetic domain.

The long-lived Davis-Greenstein *magnetic relaxation* (Davis & Greenstein 1951; Purcell 1979; Roberge & Lazarian 1999; Das et al. 2010) is still invoked in the literature of dust alignment, though it was realized early that normal conditions in the ISM could not allow for dust alignment through this process (Jones & Spitzer 1967; Purcell 1979). We present it for its historical interest and for its simplicity.

When the grain spin axis is not aligned with \mathbf{B} , \mathbf{B} is seen as a rotating field in the body frame. In that frame, \mathbf{B} can be decomposed into a constant field \mathbf{B}_{\parallel} parallel to the main axis of inertia, \hat{a} , and a rotating field, \mathbf{B}_{\perp} , perpendicular to \hat{a} . The paramagnetic grain placed in the constant field \mathbf{B}_{\parallel} will magnetize with \mathbf{M}_{\parallel} parallel to \mathbf{B}_{\parallel} , therefore to \hat{a} . On the contrary, the rotating field \mathbf{B}_{\perp} will drag a magnetization \mathbf{M}_{\perp} along the rotation, and *with a lag behind*³ the inducing field \mathbf{B}_{\perp} . This lag characterizes the delay for the alignment of the spins of the material with \mathbf{B}_{\perp} , and is responsible for a dissipation of energy through *magnetic absorption*⁴. Because of this lag there exists a component of \mathbf{M}_{\perp} perpendicular both to \hat{a} and \mathbf{B} . We note it $M_{\perp}^{\hat{a},\mathbf{B}}$.

The total magnetic torque controlling the variation of the angular momentum \mathbf{J} , $\mathbf{M} \times \mathbf{B}$, has three components. One is antiparallel with \hat{a} , $\mathbf{M}_{\perp}^{\hat{a},\mathbf{B}} \times \mathbf{B}_{\perp}$, and tends to reduce J , and therefore to slow down the grain, dissipating the rotational energy through magnetic absorption. Another is perpendicular to \hat{a} and therefore to \mathbf{J} , $\mathbf{M}_{\perp}^{\hat{a},\mathbf{B}} \times \mathbf{B}_{\parallel}$, and *directed towards* \mathbf{B} . This component modifies the direction of \mathbf{J} without affecting its amplitude, progressively aligning⁵ the grain spin axis with \mathbf{B} . The remaining component, $(\mathbf{M} - \mathbf{M}_{\perp}^{\hat{a},\mathbf{B}}) \times \mathbf{B}$, which

3. In the grain frame, the magnetic field is rotating in the opposite direction of the grain spin. The magnetization \mathbf{M}_{\perp} lies therefore ahead of \mathbf{B}_{\perp} , following the rotation of the grain.

4. The amount of heat dissipated is determined by the imaginary part of the complex magnetic susceptibility of the material.

5. Just like the friction torque for the spinning top, it is the same component of the magnetization, $M_{\perp}^{\hat{a},\mathbf{B}}$, which is responsible both for the slowing down of the grain through magnetic absorption and for its alignment along \mathbf{B} .

is perpendicular both to \mathbf{J} and \mathbf{B} , makes the grain precess around \mathbf{B} . The magnetization induced by the Barnett effect, being parallel to \mathbf{J} , only affects the precession of the grain with no effect on alignment.

Predictions of the theory Das et al. (2010) recalls the predictions of the Davis-Greenstein *magnetic relaxation* theory. We note T_d the dust temperature, T_g the gas temperature, and n_H the proton density.

- The imperfect Davis-Greenstein mechanism gives a full description of the grain precession dynamics, through the probability distribution of the precession angle β , as a function of an alignment parameter ξ :

$$f(\beta, \xi) = \frac{\xi \sin \beta}{(\xi^2 \cos^2 \beta + \sin^2 \beta)^{3/2}} \quad (2.4)$$

Alignment is perfect when ξ is zero, and approaches random alignment when ξ is close to 1 or higher.

- The maximal grain size aligned by magnetic relaxation is defined through the parameter δ_0 . It increases with the magnetic field intensity and the imaginary part, χ'' , of the complex susceptibility χ controlling magnetic dissipation. It decreases with increasing gas collision rate which tend to disalign grains. δ_0/a is, for the grain of radius a , the ratio of the gas disaligning timescale to the magnetic aligning timescale (Hong & Greenberg 1980).

$$\delta_0 = 8.23 \cdot 10^{23} \frac{\chi'' B^2}{n_H T_g^{1/2} T_d} \mu\text{m} \quad (2.5)$$

The intensity of the magnetic field needed to explain starlight polarization with paramagnetic relaxation is $B \sim 2 \times 10^{-5}$ G (Jones & Spitzer 1967). In the diffuse ISM, this corresponds to δ_0 of the order of $0.2 \mu\text{m}$ (Hong & Greenberg 1980; Das et al. 2010). The use of ferromagnetic or superparamagnetic particles (paramagnetic matrix containing clumps of ~ 100 iron atoms each) would increase χ'' and subsequently alleviate the need for a high magnetic field, allowing a sufficient alignment with $B \sim 10^{-6}$ G (Jones & Spitzer 1967).

- The alignment parameter ξ depends on the grain size a through the following expression :

$$\xi^2(a) = \frac{a + \delta_0 (T_d/T_g)}{a + \delta_0} \quad (2.6)$$

As a increases, $\xi(a)$ approaches unity as soon as $a \sim \delta_0$. From this we infer that magnetic relaxation better aligns small grains than large grains. As long as the dust temperature is much lower than the gas temperature, increasing δ_0 can increase the maximal size of aligned grains.

2.3.3 Radiative alignment : the radiative torques (RATs)

The model of *radiative torques* (RATs), which has become for a decade the favoured alignment process thanks to its thorough theoretical development (Draine & Weingartner 1997;

Lazarian & Hoang 2007) and its confrontation to observations is at first sight surprising : it states that it is the torque produced by the absorption and scattering of stellar light that is not only spinning up the grains but also aligning them along \mathbf{B} ! Draine & Weingartner (1997) demonstrated that, for paramagnetic grains, the radiative torques are more efficient in aligning dust grains along the magnetic field than the Davis-Greenstein magnetic relaxation torques.

Anisotropy of the radiation field Through their momentum, photons can exert radiative torques onto dust grains. If the radiation field was strictly symmetric, which is certainly not the case in reality, radiative torques would not produce any aligning effect (Draine & Weingartner 1997). The radiation field must be at least partially anisotropic. We decompose it into an isotropic and an anisotropic component, and concentrate on the effect of the anisotropic component.

Grain helicity If the grains were aspherical but perfectly symmetric like prolate (cigars) or oblate (pancakes) spheroids, which they are certainly not, it can be shown that the radiative torque, Q_{e3} as per Lazarian & Hoang (2007), would make the grain precess in the plane perpendicular to the direction of the radiation field, without any effect on its spinning or alignment. If we assume that grains are asymmetric, with an *helicity* defined as a different absorption/scattering cross-section for left and right circularly-polarized light, then two new components of the radiative torques, Q_{e1} and Q_{e2} , appear to be able to spin-up⁶ the grains and to align them along the magnetic field if the ratio $Q_{e1}^{\max}/Q_{e2}^{\max}$ is sufficiently large (Lazarian & Hoang 2007). This effect is only produced by the anisotropic component of the radiation field, while the effect of the isotropic component is similar to that of H_2 torques.

Low-J and high-J attractor points Lazarian & Hoang (2007) found that the effect of RATs pushed the grain spinning towards 2 attractor points in the plane (angular momentum) *versus* (alignment angle between \mathbf{J} and \mathbf{B}) : a low-J attractor (with an angular momentum J of the order of its thermal value J_{th}), and a high-J attractor (with $J \gg J_{\text{th}}$). The high-J attractor corresponds to a perfect alignment of the grain around the magnetic field lines, while the low-J attractor corresponds to an imperfect alignment (with a loss in the alignment estimated to be $\sim 20-30\%$, Hoang et al. 2013). In practice, a grain is considered to be aligned if its rotational velocity is higher than 3 times its thermal rotational velocity :

$$\frac{\omega}{\omega_{\text{thermal}}} > 3 \quad (2.7)$$

In the RATs theory, the existence of high-J attractor, therefore the perfect alignment of grains, is primarily determined by the value of the ratio of the maximal values of the two torques $Q_{e1}^{\max}/Q_{e2}^{\max}$, a function of the grain size, shape, composition and helicity. But it also depends on the radiation field (its intensity, factor of anisotropy), on the gas density and

6. Pinwheel torques from H_2 formation depend on the repartition of chemical sites at the surface of grains, and are therefore short-lived. On the contrary, RATs depend on the grain shape and can be long-lived (Lazarian & Hoang 2007).

temperature, on the angle between the magnetic field and the direction of the anisotropic component of the radiation field. [Hoang & Lazarian \(2008\)](#) demonstrate a counter-intuitive result, that gaseous bombardment can align grains by kicking grain out of a low-J attractor to a high-J attractor.

Predictions of the theory The radiative torque theory has predictions distinctive from that of the magnetic relaxation ([Lazarian & Hoang 2007](#); [Hoang et al. 2014](#)).

- Dust alignment should improve when the radiation field intensity increases, at least for its anisotropic component. Correlations of dust alignment with the distance to neighbouring stars, or with dust temperature, are therefore expected.
- The magnitude of the RATs efficiency depends on the ratio of the grain radius with the wavelength of the radiation ([Lazarian & Hoang 2007](#))

$$Q_{\Gamma} \simeq 0.4 \left(\frac{\lambda}{a} \right)^{\eta} \quad (2.8)$$

with $\eta = 0$ for $\lambda \leq 2a$ and $\eta = -3$ for $\lambda \gg a$. The RATs efficiency therefore decreases very fast with the wavelength, and is maximal when scattering dominates over absorption. There are at least two consequences : 1) small grains should be less aligned than large grains in the diffuse ISM dominated by the ISRF, and 2) the RATs become less efficient at high optical depths where the UV and optical part of the radiation field is extinguished. One therefore expects a decrease of the polarization fraction with the column density.

- Similarly to windmills, grains are driven to higher velocities when the radiation field "blows" facing the grains, than from the side. The alignment efficiency of the radiative torque depends on the angle, ψ , between the direction of the magnetic field and the anisotropic component of the radiation field. It is maximal when the radiation field anisotropy is parallel to \mathbf{B} , and null when it is perpendicular to \mathbf{B} (*e.g.*, [Hoang et al. 2014](#)) :

$$J_{\max}^{\text{RAT}}(\psi) = J_{\max}^{\text{RAT}}(\psi = 0) \cos \psi \quad (2.9)$$

- In the absence of magnetic field, or if the precession caused by the radiative torque Q_{e3} was faster than the magnetic (Larmor) precession, dust grains should align along the radiation field anisotropy, and not along \mathbf{B} ([Lazarian & Hoang 2007](#))! This however necessitates a very strong radiation field ($G_0 \sim 10^3$,) that is rarely encountered in the ISM, but is encountered close to giant stars.

Confrontations of RATs with observations The radiative torque model was initially the only mechanism able to explain how dust polarization could still be observed in dense clouds. In the magnetic relaxation paradigm (Section 2.3.2), dust grains should indeed not be aligned anymore at high densities because $T_{\text{gas}} \simeq T_{\text{dust}}$. In the radiative torque paradigm, NIR photons, which are not extinguished so efficiently like UV photons, are still able to align large ($a \sim \lambda$) grains.

In the recent years, the radiative torque model has been extensively developed, with clear predictions (see previous paragraph). There have been many claims about the successful

confrontation of the radiative torque theory with observations, which are summarized in the reviews by [Andersson et al. \(2015\)](#) and [Andersson \(2012\)](#).

2.3.4 Mechanical alignment : alignment in gas flows

[Gold \(1952\)](#) has demonstrated that dust grains could also be aligned by supersonic gas flows. This theory has been recently revised in the context of helical grains, for subsonic flows. It has been shown that, similarly to radiative torques, the anisotropic motion of gas would produce mechanical torques able to align the grains along the flow in the absence of magnetic field, and along \mathbf{B} if the precession of the grain is dominated by the Larmor precession around \mathbf{B} ([Lazarian & Hoang 2007](#)).

2.3.5 Other subtleties in the grain alignment dynamics

Alignment of graphite grains The high level of anisotropy of graphite conducted [Cayrel & Schatzman \(1954\)](#) to propose that graphite flakes, which are easily formed in the laboratory and could therefore exist in the ISM, could be responsible for the polarization of starlight. Owing to the strong intrinsic polarization of graphite flakes, the grain alignment would not need to be strong to explain observations. Paramagnetic impurities or diamagnetism could produce a magnetic relaxation sufficient to align those grains under a weak magnetic field intensity ($B \sim 10^{-6}$ G, [Jones & Spitzer 1967](#)).

Cross-overs If the torque driving the suprathreshold rotation never changed sign, the alignment process would slowly but surely align grains perfectly, and not imperfectly as is always the case with thermal rotation (classical Davis-Greenstein process). Perfect alignment would allow to invoke simple paramagnetic materials, embedded in a magnetic field of a reasonable intensity. But this can not be insured if the spin-up torque changes its sign during the alignment process, as it is the case for H_2 torques which are exerted on *short-lived* chemical sites on the surface of the grain. Cross-overs are those moments in the grain dynamics when the angular momentum \mathbf{J} goes through zero before increasing again, possibly losing the memory of its previous direction. This randomization happens through a random walk induced by disaligning torques (gas bombardment), which become more efficient when J is close to its thermal value ([Spitzer & McGlynn 1979](#)). [Spitzer & McGlynn \(1979\)](#) have examined in detail the dynamics of cross-overs. They find that the typical timescale between 2 cross-overs is uncertain, but much shorter than the alignment timescale through magnetic relaxation. The angular momentum before and after the cross-over turns out to be correlated, but this correlation is insufficient to achieve significant alignment through magnetic relaxation. Frequent cross-overs would then prevent any alignment by magnetic dissipation.

[Lazarian & Draine \(1997\)](#) have reexamined this scenario, relaxing the assumption of internal alignment (\mathbf{J} aligned with \hat{a}) made by [Spitzer & McGlynn \(1979\)](#). This assumption was reasonable as the timescale for internal alignment through the Barnett effect is much short than the timescale for alignment. But this disregarded thermal fluctuations in the magnetization⁷. Because of thermal fluctuations in the magnetization, \mathbf{J} and \hat{a} are close

7. Which are also responsible for the magnetic dipole emission of grains ([Draine & Hensley 2013](#)).

but never perfectly aligned. This tiny difference becomes critical during cross-overs when J is also tiny, and diminishes the randomization of \mathbf{J} at the cross-over. They find that grains larger than $\sim 0.15 \mu\text{m}$ would be perfectly aligned, while smaller grains would be only partially aligned. This threshold was revised to $1 \mu\text{m}$ when nuclear relaxation, a process more efficient than the Barnett effect, is included (Lazarian & Draine 1999). If the reader still follows, this means that grains could not be aligned by magnetic relaxation due to cross-overs.

Unlike pinwheel torques, radiative torques do not change sign through a cross-over (Lazarian & Hoang 2007). As a consequence, pinwheel torques tend to spin-up the grain after a cross-over, while RATs continue to drive the momentum J to zero. Cross-overs would then be a problem for the alignment of dust grains by RATs. However, Hoang & Lazarian (2008) showed that, for a ellipsoid shape with 3 different axis, no drive to zero is observed, but rather a low- J attractor point at thermal velocity.

Thermal flipping and thermal trapping These processes are important for the alignment of small ($a \leq 0.1 \mu\text{m}$) grains. Thermal fluctuations tend to disalign \mathbf{J} and \hat{a} (Lazarian & Draine 1997), while still conserving \mathbf{J} . Lazarian & Draine (1999) show that during a cross-over, a small grain undergoing thermal fluctuations can have its axis of maximal inertia \hat{a} rotate while conserving \mathbf{J} : this is a *thermal flip*. The cross-over has been bypassed, with a minimal angular momentum through the cross-over that is higher than without flipping, thus limiting the randomization of \mathbf{J} (Spitzer & McGlynn 1979). With thermal flipping, small grains rotating supra-thermally would remain perfectly aligned even through cross-overs.

This is however not the full story. Small grains will be subject to very frequent thermal flipping, because the Barnett effect insuring the internal alignment of \mathbf{J} and \hat{a} is less efficient than the disaligning collisions with gas particles for small grains than for large grains. This frequent thermal flipping, which prevents any suprathemal rotation of small grains, is called *thermal trapping*. The net alignment of small grains will result from the competition of thermal trapping with aligning and speed-up processes like RATs and pinwheel torques, which makes the minimal size of aligned grains depend on the environment.

The reader, together with the author of these lines, will probably admit that the complexity of the dust alignment physics is hard to follow.

2.4 Observational constraints from dust polarization

Observations of dust polarization brings informations on the structure of the Galactic magnetic field as well as specific constraints to dust models, that we summarize here.

2.4.1 Spectral information

Spectral dependence of p (the Serkowski's Curve)

In the diffuse ISM, the spectral dependence of the polarization degree of starlight, the interstellar polarization curve $p(\lambda)$, has a peak in the visible close to the V band, and falls off toward both the infrared and the UV (*e.g.* Serkowski et al. 1975; Andersson & Potter 2007). By contrast, the interstellar extinction curve $\tau(\lambda)$ decreases with the wavelength from

the UV to the infrared (*e.g.*, Fitzpatrick & Massa 2007). From this combination it is inferred that small grains are either spherical or not aligned (Mathis 1986; Kim & Martin 1995) and that the polarization is dominated by "large" grains (around $0.1 \mu\text{m}$ in size, *e.g.* Draine & Li 2007). Nevertheless, Das et al. (2010) demonstrate that the $p(\lambda)$ curve can be well fitted with small grains ($a \sim 0.01 - 0.05 \mu\text{m}$) still moderately aligned.

The following expression⁸ has been shown to successfully fit $p(\lambda)$ in the optical (Serkowski et al. 1975) :

$$p(\lambda) = p_{\text{max}} \exp^{-K \log^2\left(\frac{\lambda}{\lambda_{\text{max}}}\right)} \quad (2.10)$$

with some departures in the infrared (power-law, Martin et al. 1992) and in the UV (super-Serkowski behavior, Martin et al. 1999)

The peak of the polarization curve, λ_{max} , characterizes the minimal size in the aligned grain population. It is thought to be the most robust diagnostic for dust alignment (see Section 2.4.2), much better than the highly degenerated polarization fractions p/τ or P/I .

Polarization in absorption bands

Polarization of absorption bands shows that silicate grains are aspherical and aligned (Dyck & Beichman 1974), but that aliphatic carbon grains, responsible for the $3.4 \mu\text{m}$ band, are not (Adamson et al. 1999; Chiar et al. 2006). The CO and H₂O bands of the ice coatings covering grains are also polarized (Whittet et al. 2001; Hough et al. 2008). The 220 nm absorption bump, attributed to very small carbon aromatic particles, is not seen in polarization, with the exception of 2 lines of sight (Anderson et al. 1996; Martin et al. 1999; Hoang et al. 2013). However, the question of whether the large aromatic carbon grains used in dust models (Draine & Li 2007; Compiegne et al. 2011) are aligned or not is not directly constrained by such observations because of the lack of characteristic bands.

Circular polarization

Starlight is also circularly polarized by dust extinction, if the magnetic field rotates along the line of sight. This is a second order effect revealing the *birefringence* of the ISM (Mathewson & Ford 1971; Siebenmorgen et al. 2014). The wavelength dependence of starlight circularly polarization is related to that of its linear polarization (Martin & Angel 1976).

Ground observations from the wavelength dependence of dust polarized emission

Well before *Planck*, It was possible to observe dust polarized emission in star-forming regions from the ground. These environments are quite different from the diffuse ISM, with a much higher radiation field and much higher densities. Most of those studies have been conducted to map the magnetic field, in its relation to star formation (*e.g.*, Poidevin et al. 2013)

Multi-wavelength observations also allowed to characterize the wavelength dependence of the dust polarization fraction P/I . Its shape is complex, with a minimum around $300 \mu\text{m}$, which necessitates "a model in which the emission arises from dust grains at multiple

8. This is *not* a log-normal.

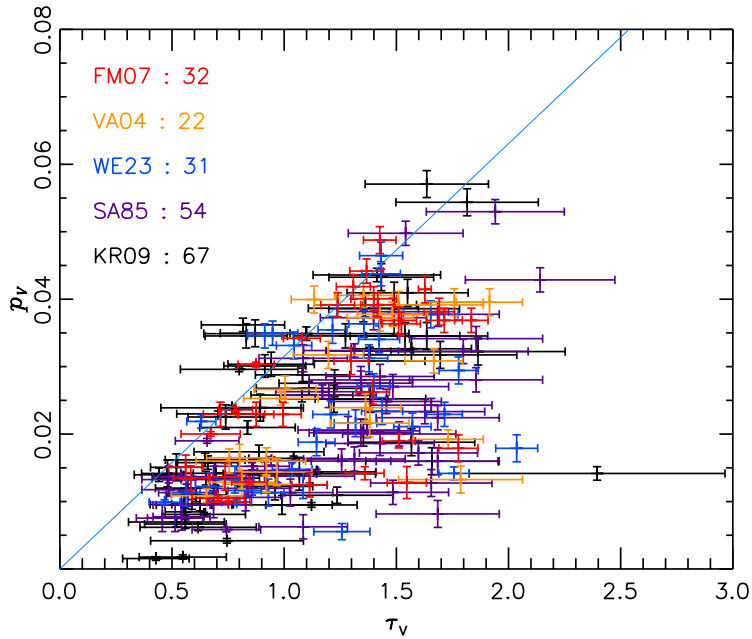


FIGURE 2.2 – Scatter plot of the starlight polarization degree in the optical p_V with the extinction A_V in the V band, for the 206 selected stars from [Planck Collaboration Int. XXI \(2015\)](#). The blue line is the upper envelop $p_V \leq 9 E(B - V)$ of [Serkowski et al. \(1975\)](#)

temperatures along the line of sight and in which the polarizing efficiency of these grains is correlated with their temperature" ([Vaillancourt 2002](#)). According to [Zeng et al. \(2013\)](#), these observations supports the idea of the RATs mechanism, which drives a higher alignment efficiency in the region that is exposed to a stronger radiation field.

2.4.2 Observational constraints on dust alignment

On this subject, the reader is also refered to the more complete reviews by [Andersson \(2012\)](#) and [Andersson et al. \(2015\)](#).

Maximal fraction of polarization observed in the optical

The maximal fraction of polarization observed in the visible is the upper envelop of the scatter plot $p = f(\tau)$ in the V band : $p \leq 9 E(B - V)$ ([Serkowski et al. 1975](#)), corresponding to $p/A_V \leq 3\%$ (see Fig. 2.2). Variations in the magnetic field geometry and in the dust alignment efficiency contribute to the variation of p , so that the upper enveloppe of this scatter plot should correspond to the particular case of optimal alignment both for the magnetic field and for the grains.

Correlation of polarization with elemental depletions

[Voshchinnikov et al. \(2012\)](#) have studied the correlation of p and p/τ with elemental depletions of Mg, Fe and Si. These elements enter in the constitution of silicate grains,

which are known to be aligned, and of iron-bearing species for which the question is still open. They found that "the increase of the iron content in non-silicate grains does not enhance polarization", which excludes iron-bearing species as a dominant polarization carrier. They also found a strong correlation between p and the depletion of Si, as one would expect if interstellar polarization was dominated by silicates.

This study, which makes use of many lines of sight through the ISM at various longitude and latitudes, does not discuss the possibility that such trends could be related to latitude effects and ultimately to the geometry of the Galactic magnetic field.

Constraining the typical size of aligned grains with λ_{\max}

The wavelength λ_{\max} of the peak of the polarization curve in the optical is a measure of the typical size of aligned grains. Unlike other polarization tracers, It has the clear advantage of being independent of the structure of the magnetic field. Still, λ_{\max} can vary through different physical processes. In the frame of radiative torques, it is the radiation field (its spectrum, its intensity, anisotropy and direction with respect to the magnetic field) that controls the minimal size of aligned grains, and therefore λ_{\max} (Andersson & Potter 2007). But λ_{\max} would also trace the growth of aligned grains through coagulation (Vrba et al. 1993; Wurm & Schnaiter 2002). Both models predict an increase of λ_{\max} with A_V .

Traps in the interpretation of p_V/A_V and P/I in terms of grain alignment

The decrease with the column density of the dust polarization fraction observed in the optical and NIR has been characterized in many papers well before *Planck* (e.g. Goodman et al. 1995; Gerakines et al. 1995; Whittet 2004; Whittet et al. 2008; Chapman et al. 2011). It is a general property of dust polarization. Note that there are however some exceptions where p_V/A_V increases with A_V (e.g. Jones 2003).

In the literature, the complexity of the physics driving the value of the polarization fraction p_V/A_V is often over-simplified. With a few exceptions (e.g. Jones et al. 1992, 2015; Chapman et al. 2011), it is still usually interpreted as a direct measure of the grain alignment efficiency (e.g. Whittet et al. 2008; Andersson 2012; Voshchinnikov et al. 2012; Cashman & Clemens 2014), whereas it depends also on the magnetic field structure, as well as the dust size, shape and optical properties.

Another factor is rarely mentionned. Dust grains are subject to an evolutionary process in the diffuse ISM, and even more when entering dust clouds (see Chapter 1). This is characterized by an increased emissivity, and is associated to grain growth. Dust grains at an A_V of ~ 10 are not diffuse dust grains, in size, shape and in optical properties. Why should their polarization efficiency be the same? There is no reason to ignore such a big change in the properties of the carriers of polarization when trying to correlate polarization and extinction in cores.

2.5 Dust models satisfying these pre-Planck constraints

Various models of diffuse dust have been developed to reproduce the polarization and extinction spectral dependences, as well as the dust thermal emission, with a combination

of aligned and unaligned grains (*e.g.* Lee & Draine 1985; Li & Greenberg 1997; Draine & Fraisse 2009; Voshchinnikov 2012; Siebenmorgen et al. 2014).

Models with only silicate grains aligned can reproduce the observations, even with a moderate elongation (≥ 1.5) if we allow for an almost perfect alignment of large silicate grains (*e.g.* Martin 2007; Draine & Fraisse 2009). It is also possible to satisfy those constraints by aligning both silicate and carbon grains (Draine & Fraisse 2009), thus resulting in a lower alignment of grains. Models predict a polarization fraction $\sim 10 - 13\%$ in the submillimeter (Martin 2007; Draine & Fraisse 2009), consistent with the observations at $100 \mu\text{m}$ in Galactic clouds from the Kuiper Airborne Observatory (Hildebrand et al. 1995), but only marginally with those at $850 \mu\text{m}$ of the Archeops Balloon (Benoît et al. 2004) which prefigured the *Planck* mission.

Chapitre 3

Statistical properties of dust polarized emission as seen by *Planck*

With *Planck*, we had to learn collectively how to handle polarization data, which differ from intensity maps through many aspects.

3.1 Manipulating full-sky polarization data

The Stokes formalism gives the possibility to describe the polarization of an electromagnetic wave, elliptical in the general case, through 4 parameters : I (the total intensity), Q and U (which characterize its linear polarization), and V (for its circular polarization). Because the physical processes responsible for the CMB emission can not produce circular polarization, *Planck* was designed without any capacity to measure Stokes V ⁹.

How does *Planck* HFI measure Q and U? The Stokes parameters Q and U can be retrieved from the measure of the polarized intensity along 4 orientations, each rotated by 45° . To achieve this, the *Planck* HFI instrument relies on pairs of Polarization Sensitive Bolometers (PSB) rotated by 45° with respect to each other. Each bolometer is able to measure the polarized intensity in two perpendicular directions, through a grid of parallel and perpendicular wires. Some instrumental polarization is created by the difference in the transmitting spectra of each bolometer in the pair, a nuisance called *spectral mismatch*, which can be partially corrected using pre-launch ground measures of the transmission spectras, or through in-flight calibration techniques.

Q and U are spin-2, algebraic quantities Handling the intensity maps is easy, but not the Q and U maps. Q and U stokes parameters are not scalar but spin-2, algebraic, quantities, which are not independent from each other¹⁰. The Stokes parameters Q and U also depend on the local referential on the sphere represented by the local meridian and parallel. As

9. Dust emission is also expected not to be circularly polarized. Nevertheless, the linear polarization of CO bands by the Goldreich-Kylafis effect (Goldreich & Kylafis 1981) could produce circular polarization in CO-bands through optical depths effects (Houde et al. 2013).

10. Unlike I maps, Q and U can not be stacked without loosing information.

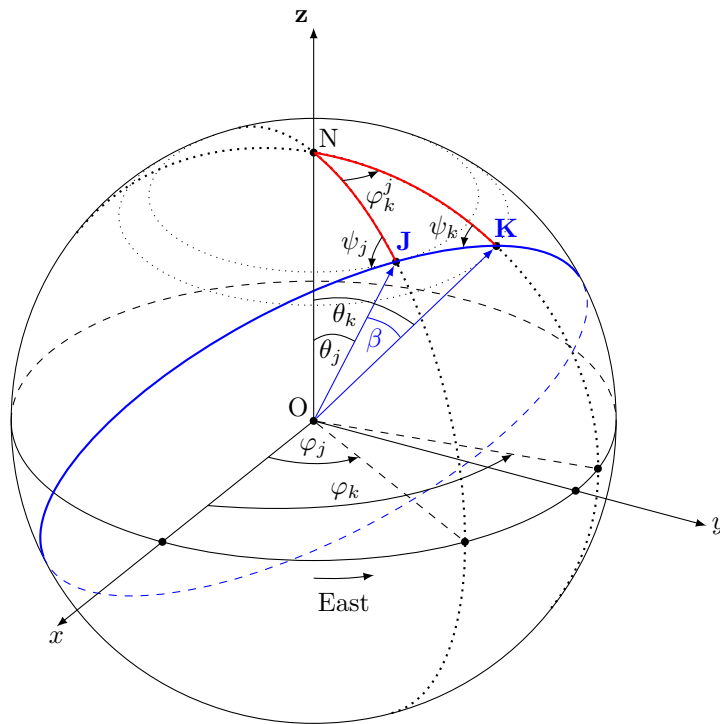


FIGURE 3.1 – Definition of points and angles on the sphere involved in the geometry of the smoothing of polarization maps (adapted from Keegstra et al. (1997)). J is the position of the centre of the smoothing beam, and K a neighbouring pixel, with spherical coordinates (φ_*, θ_*) and (φ_k, θ_k) , respectively. The great circle passing through J and K is shown in blue. The position angles ψ_* and ψ_k here are in the HEALPix convention, increasing from Galactic north toward decreasing Galactic longitude (west) on the celestial sphere as seen by the observer at O. From Planck Collaboration Int. XIX (2015).

shown on Fig. 3.1, Q values at points J and K can not be directly correlated or combined because they were measured in a reference frame which does not have the same orientation. This has implications for the correlation analysis, for the smoothing of Q and U maps, as well as for the derivation of the covariance matrix at lower resolution from its knowledge at full resolution. See Appendix A from Planck Collaboration Int. XIX (2015) for more information.

From the measure of Stokes parameters Q and U , one can infer the following observables of dust polarization :

Polarization intensity

$$P = \sqrt{Q^2 + U^2} \quad (3.1)$$

Unlike Q and U , the polarization intensity P is a scalar and therefore independent of any reference frame. Unfortunately, through the noise affecting Q and U , the quantity Q^2 and U^2 are positively biased, and so is P . Different techniques, or estimators, allow to reduce this bias (Simmons & Stewart 1985; Plaszczyński et al. 2013; Montier et al. 2015), but it can never be totally removed from P . When it is possible, it is recommended to work in Q and U , which are unbiased quantities, and not in P . This is especially important for any correlation analysis (Planck Collaboration Int. XXI 2015; Planck Collaboration Int. XXXII 2014). If

working with P is necessary, smoothing the data decreases the noise, and at the same time, the bias. When smoothing is not possible, selecting high signal-to-noise data (larger than 3 or 4) limits the problem because all estimators converge to the same correction factor when the SNR is larger than 4 (Simmons & Stewart 1985). Because of this bias, stacking low-SNR polarization data in P is complicated, because we then also stack the bias.

Polarization angle in the IAU convention

$$\psi = 0.5 \arctan(-U, Q) \quad (3.2)$$

The polarization angle, ψ , is given for a particular frame of reference (equatorial, galactic) and with a sign convention¹¹. Assuming that the magnetic interpretation is correct, the direction of starlight polarization is parallel to the plane-of-the-sky projection of the magnetic field, while that of polarized emission is perpendicular to it. Unlike P , ψ is not a biased quantity, through its statistics is not gaussian if the SNR is too weak (Naghizadeh-Khouei & Clarke 1993).

3.2 Statistical properties of dust polarized emission from the *Planck* HFI 353 GHz channel

The 353 GHz channel is the polarization-sensitive HFI channel with the highest frequency, and therefore the highest signal-to-noise ratio. Two *Planck* Intermediate Results articles concentrated on the analysis of the statistical properties of dust polarized emission, and of the underlying magnetic field (Planck Collaboration Int. XIX 2015; Planck Collaboration Int. XX 2015). Here are some of their results.

Despite the 5' resolution of the 353 GHz channels, maps had to be degraded to a resolution of 1° to reach a reasonable SNR in the most diffuse parts of the Galaxy and therefore limit the bias in P . Very diffuse regions where the data systematics were not fully understood were masked. The map of the polarization fraction P/I revealed bright structures unknown to us, sometimes with no clear counterpart in the corresponding intensity map (Fig. 3.2) : among others the so-called Fan region ($l \sim 150^\circ$), well known from synchrotron observations, the Aquila Rift, and some regions for which we had to find a name like Ara and Pavo. The polarization fraction tends to be the highest in the most diffuse regions or envelopes surrounding molecular clouds. The Galactic plane is strongly depolarized. Dense clouds and cores appear as polarization holes (Ophiucius, Taurus, Musca), as it was long known from starlight polarization in the NIR (see Section 2.4.2).

What is really new with Planck is the observation of the most diffuse area of the galaxy, more difficult to observe in extinction. In those regions, P/I can reach values as high as 20%, though in a very small fraction of the sky. This was not fully unexpected after the observations of Archeops (Benoît et al. 2004), but no dust models could explain at that time such high values (e.g. Martin 2007; Draine & Fraise 2009).

11. *Planck* data are provided in the form of full-sky HEALPix maps (Gorski et al. 1999). In this convention, polarization angles increase to the West, in opposition to the IAU convention where angles increase to the East. The minus sign in front of U in Eq. 3.2 allows to change from the HEALPix to the IAU convention.

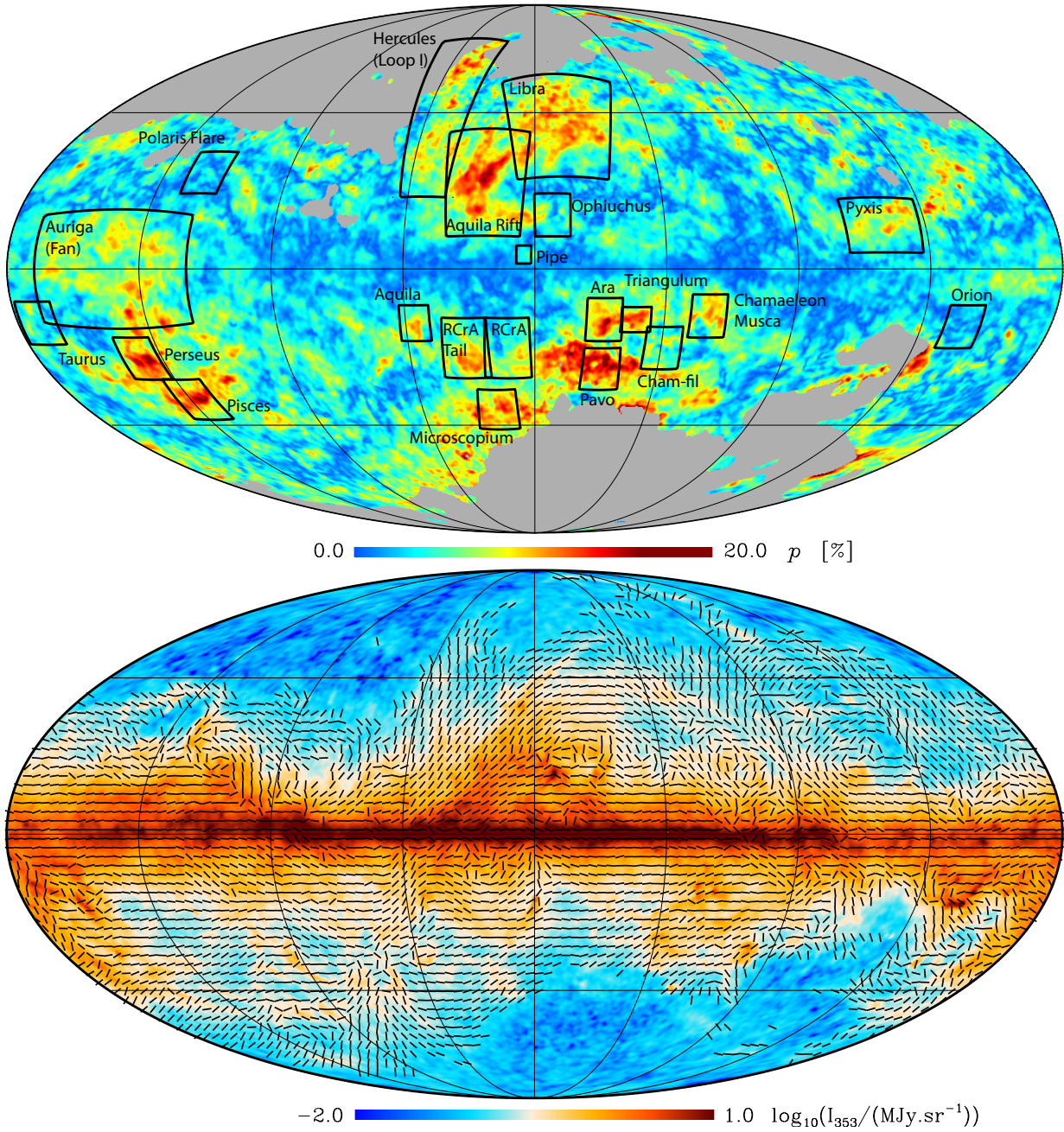


FIGURE 3.2 – (Top) Map of the polarization fraction P/I at 353 GHz at a resolution of 1° , debiased with the [Montier et al. \(2015\)](#) bayesian method. (Bottom) Map of the 353 GHz polarization angles rotated by 90° . Regions dominated by systematic instrumental effects were masked. From [Planck Collaboration Int. XIX \(2015\)](#).

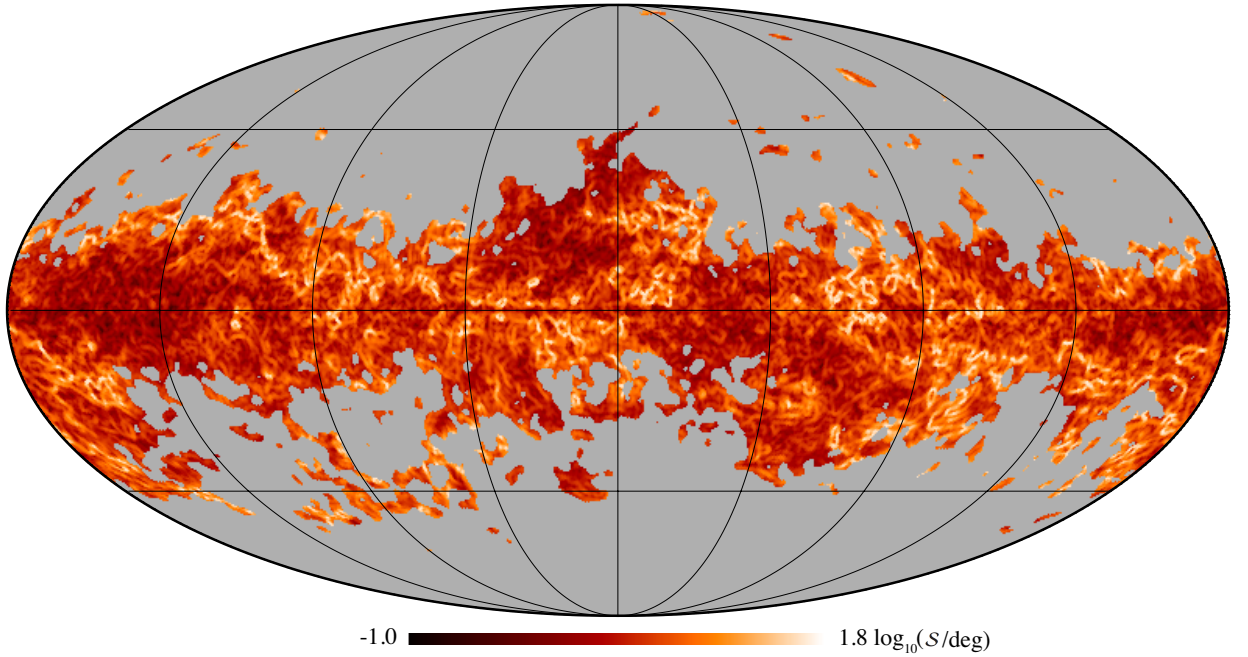


FIGURE 3.3 – Map of the angle structure function, S , at 353 GHz and at a 1° resolution ($\Delta\delta = \delta = 30'$). The derived S in masked regions is too noisy to be reliable. From [Planck Collaboration Int. XIX \(2015\)](#).

3.2.1 Anticorrelation between the polarization fraction P/I and the apparent magnetic field disorder

As can be seen in Fig. 3.2, regions with high polarization fraction P/I are always associated with patches of uniform polarization angles ψ (*i.e.* ordered magnetic field, like Aquila Rift or Pavo). Regions with low polarization fractions are sometimes, not always, associated to elongated filamentary regions, sometimes tens of degrees long, where the orientation of the direction of polarization abruptly changes (through the polaris flare for example).

This relation could be quantified using the angle structure function $S(x, \delta)$, which measures at the position x the local dispersion of the polarization angles. The difference in polarization angle between pixels x and i is

$$\Delta\psi_{xi} = \psi(x) - \psi(i) = 0.5 \arctan(Q_i U_x - Q_x U_i, Q_i Q_x + U_i U_x) \quad (3.3)$$

From this we derive the angle structure function $S(x, \delta)$ by summing over all pixels i falling in the annulus centered on x , of radius δ and width $\Delta\delta$.

$$S(x, \delta) = \left(\frac{1}{N} \sum_{i=1}^N (\Delta\psi_{xi})^2 \right)^{1/2} \quad (3.4)$$

$$(3.5)$$

S emphasize those regions where ψ varies abruptly (Fig. 3.3). The structure function S , as well as the map of the gradient $\nabla P/P$ often used in studies of Faraday rotations

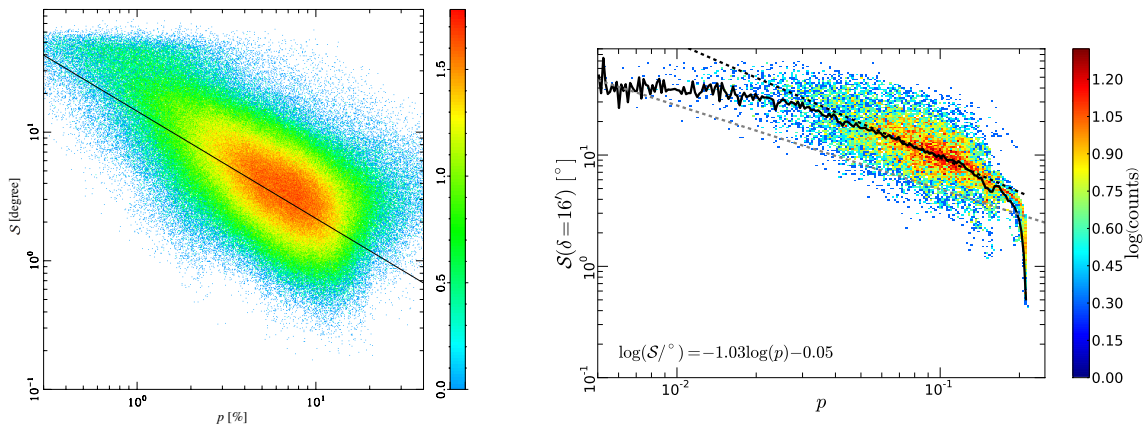


FIGURE 3.4 – Anti-correlation of $p = P/I$ with S in *Planck* data (left) and in MHD simulations (right). The fit from the left figure is reproduced on the right figure (lower dashed line). From [Planck Collaboration Int. XIX \(2015\)](#) and [Planck Collaboration Int. XX \(2015\)](#).

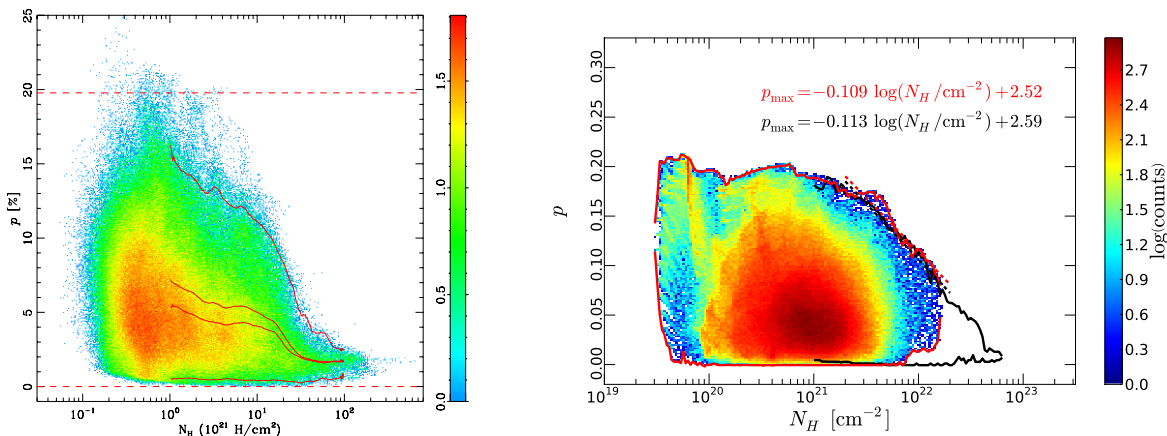


FIGURE 3.5 – Polarization fraction $p = P/I$ as a function of the gas column density, in *Planck* data at 353 GHz (left) and in MHD simulations (right). From [Planck Collaboration Int. XIX \(2015\)](#) and [Planck Collaboration Int. XX \(2015\)](#), respectively. See text for comments.

([Iacobelli et al. 2014](#)), were found to be both clearly anticorrelated with P/I (Fig. 3.4), though with a noticeable dispersion. This had already been observed before *Planck* ([Hatano et al. 2013](#)), and is confirmed in the recent BlastPOL paper ([Fissel et al. 2015](#)). We were able to reproduce this trend in a MHD simulation ([Planck Collaboration Int. XX 2015](#)), though with a clear offset (Fig. 3.3). This difference indicates that the MHD simulation used in this paper produces a magnetic field which is too tangled with respect with observations. As a consequence, it produces too much depolarization, leaving some rooms for other processes such as a loss of grain alignment to explain the decrease of P_{353}/I_{353} with the column density.

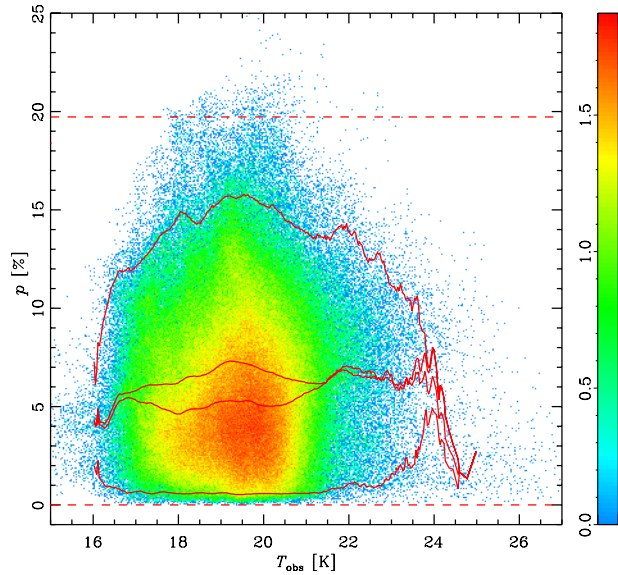


FIGURE 3.6 – Polarization fraction P/I at 353 GHz, as a function of the grain temperature inferred from a fit to the dust SED. In red from the top to the bottom are the upper 1% percentile, the mean and the median, and the lower 1% percentile. From [Planck Collaboration Int. XIX \(2015\)](#).

3.2.2 Decrease of P/I with increasing column density

At all column densities, the values of the fraction of polarization spans the full range from zero to an upper limit which was found to decrease with the column density. This was nothing new, as it had been observed long ago in starlight polarization in the optical and NIR (see Section 2.4.2). But the huge statistics brought by the *Planck* full-sky map (200,000 pixels/line of sight at a 1° resolution) was new, and brought us the large scale view on those statistics. In Fig. 3.5 one could observe a clear break, at a column density $\sim 10^{22} \text{ cm}^{-2}$ ($A_V \sim 5$), where the envelope of P/I starts to decrease faster. This drop could be related to the progressive loss of alignment of dust grains ([Whittet et al. 2008](#)), to dust evolution (variations of their optical properties in intensity and in polarization), or to the change in the magnetic field structure associated to the formation of denser structures like the dense filaments magnified by Herschel ([Arzoumanian et al. 2011](#)).

We were able to reproduce all those trends in MHD simulations ([Planck Collaboration Int. XX 2015](#)), in a model where the dust properties (alignment, optical properties) were kept fixed. We concluded that the statistics of P/I in the diffuse ISM was mainly driven by the structure of the magnetic field alone, not by variations in dust properties, at least up to the column densities probed by the MHD simulation (a few 10^{22} cm^{-2}).

3.2.3 Does *Planck* brings new constraints on dust alignment ?

It had been claimed, both from the RATs theory and from observations in starlight polarization, that the fraction of polarization should increase with grain temperature (*e.g.* [Andersson & Potter 2007](#); [Matsumura et al. 2011](#)) because the dust alignment efficiency is, in

this model, driven by the radiation field. In *Planck* data, no correlation was found between P/I and the dust temperature inferred from the *Planck* SED (Planck Collaboration XI 2014). This lack of correlation of P/I with T was also confirmed by the Blastpol study (Fissel et al. 2015), where the apparent correlation of P/I with T was entirely explained by the anticorrelation of P/I with the column density. This absence of correlation is however not a strong argument against RATs as dust temperature is not only driven by the radiation field, but also by dust evolution (Planck Collaboration XXIV 2011; Planck Collaboration Int. XXIX 2014; Fanciullo et al. 2015).

In *Planck* polarization data, it is difficult to isolate the effect of dust alignment from the effects of the magnetic field and possibly of dust evolution. In (Planck Collaboration Int. XXXIII 2015) we attempted to isolate the effects proper to dust (alignment and/or evolution) by modeling the magnetic field in local clouds through a 2-medium approach (see Chapter 4). In some cases, the magnetic field plays a role in the drop of the polarization fraction, in some other cases, there is a need for a loss of dust alignment or evolution.

Could the sudden drop in Fig. 3.5 at a column density of $\sim 3 \times 10^{22} \text{ cm}^{-2}$, be a signature of the sudden decrease of the grain alignment efficiency when entering regions screened from the radiation field, as stated by Jones et al. (2015)? This can not be excluded, but one must bear in mind that dust grains at such high column densities may have also evolved. My student Lapo Fanciullo started investigating this question by correlating polarization data in emission and extinction.

Chapitre 4

Coupling between the gas and the magnetic field

An other important part of the *Planck* Intermediate Results is devoted to the analysis of the structure of the magnetic with respect to that of the gas. Here are some results of the work by PhDs and post-docs which I was supervising with Francois Boulanger. With *Planck* maps, we have discovered the full-sky view on the magnetized ISM. We expected a very turbulent view, and we discovered a rather uniform magnetic field, well correlated with the gas structures.

4.1 Relative orientation of the magnetic field with the gas structures

Looking at the full-sky view on the orientation of the magnetic field in the diffuse ISM (Fig. 3.2), one can see that the magnetic field tends to be aligned with the gas structure, at least in the diffuse ISM. A good example is the Aquila Rift region.

[Planck Collaboration Int. XXXII \(2014\)](#) investigated this question, restricting the analysis to intermediate and high Galactic latitudes, which cover two orders of magnitude in column density, from 10^{20} to 10^{22} cm^{-2} . We showed that the magnetic field lines are preferentially aligned with gas filamentary structures in the diffuse ISM, and that this alignment is better in regions of high polarization fraction, than in regions of low polarization fractions (Fig. 4.1). Quantifying the degree of alignment, ξ , between the magnetic field and the gas filaments, we could show that ξ is not correlated with the angle structure fonction S (see Section 3.2.1), showing that the depolarization in the beam and along the line of sight does not influence this observed alignment. These correlations were interpreted through a gaussian model of a turbulent magnetic field as an effect of the projection of the 3D-orientation of the magnetic field on the plane-of-the sky. Looking at denser environments, an anti-correlation was found for ξ with the gas column density N_{H} , which is independent from the correlation of ξ with P/I , as shown by the 2D-dependence of ξ on P/I and N_{H} (Fig. 4.1, right). This means that this alignment decreases *statistically* when entering dense clouds.

These results were confirmed with a different methodology in [Planck Collaboration Int. XXXV \(2015\)](#) as illustrated by Fig. 4.2 (left). The observed smooth transition from prefe-

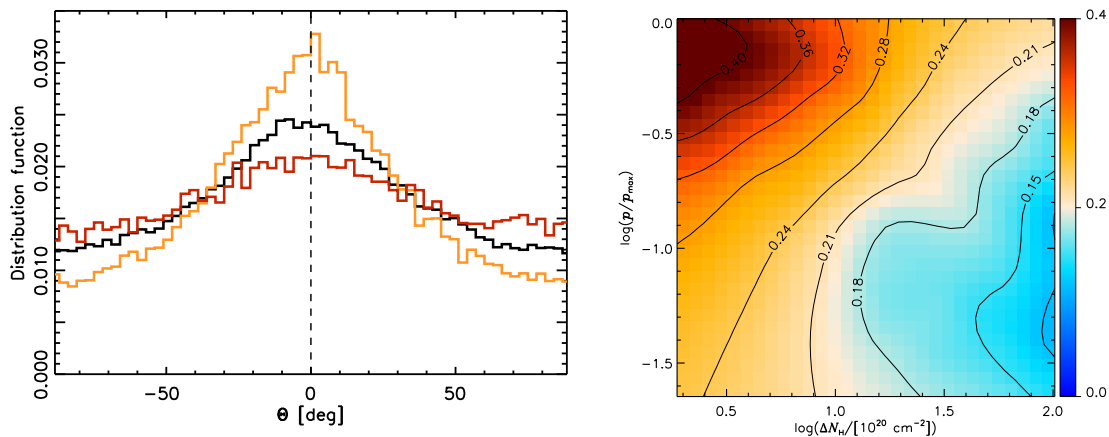


FIGURE 4.1 – (Left) Distribution function of Θ , the difference between the inferred orientation angle of the magnetic field and that of the ridges, for the selected pixels, as a function of the polarization fraction P/I of the selected structures. The black line represents all the selected pixels. The orange line refers to the pixels with the 30% highest values of P/I and the red line to the 30% lowest. (Right) 2D-dependence of the degree of alignment, ξ , between the magnetic field and the gas filaments, with the polarization fraction P/I and gas column density ΔN_{H} . From [Planck Collaboration Int. XXXII \(2014\)](#)

rentially parallel ($\xi > 0$) to perpendicular ($\xi < 0$) is similar to the transition obtained in MHD simulations for which the turbulence is Alfvénic or sub-Alfvénic. This implies that the magnetic field plays a significant dynamical role in the formation of those structures, at the scales probed by the resolution of *Planck* maps (here 10').

The global picture is that the magnetic field is significant at the scales probed by *Planck*, aligning the gas with the magnetic field in the diffuse ISM, and possibly creating perpendicular structures by gas accretion along field lines.

4.2 Structure of the magnetic field in dense structures

Two other *Planck* Intermediate Results papers concentrated on the derivation of the magnetic field structure in molecular clouds ([Planck Collaboration Int. XXXIII 2015](#)), and in star-forming regions ([Planck Collaboration Int. XXXIV 2014](#)).

In [Planck Collaboration Int. XXXIII \(2015\)](#), we analyzed the polarization data around 3 filaments (Musca, B211 and L1506 in Taurus). We showed that the magnetic field in the filament and in the background do not have the same direction. Using profiles across the filaments, we decomposed the I , Q and U Stokes parameters in the superposition of a gaussian polarized filament on a uniform polarized background. Fig. 4.3 shows our decomposition for the Musca, B211 and L1506 filaments. In the first two cases, the intrinsic dust polarization in the filaments was found to be significantly lower than in the envelope, indicating a possible loss of alignment, or an evolution of aligned grains. In L1506, the rotation of the magnetic field direction by 60° between the envelope and the filament allowed to explain the observed drop in polarization alone. This explanation in the frame of a 2-slab model is

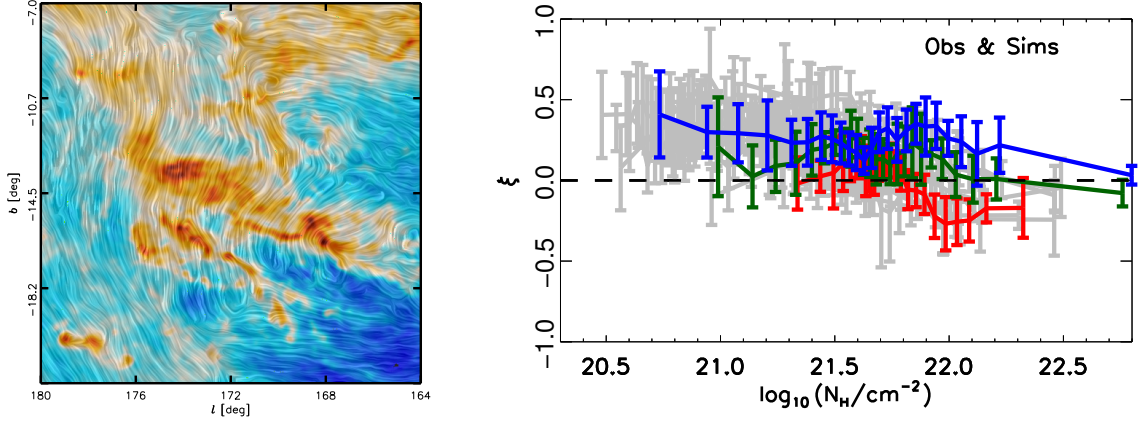


FIGURE 4.2 – (Left) Magnetic field and column density measured by *Planck* towards the Taurus MC. The colours represent column density. The drapery pattern, produced using the line integral convolution method (LIC, Cabral & Leedom 1993), indicates the orientation of magnetic field lines, orthogonal to the orientation of the submillimetre polarization. (Right) Comparison between the trends of the alignment parameter, ξ , in the synthetic observations of MHD simulations (blue for super-Alfvénic, green for Alfvénic, and red for sub-Alfvénic turbulence) and in *Planck* observations (grey for Taurus, Ophiucus, Chameleon-Musca, Lupus, CrA, Lupus, Aquila, Orion, Cepheus & IC5146), as a function of the column density N_{H} .

however not fully satisfactory for L1506 as some particular features, the severe drop of the polarization fraction outside of the filament, can not be explained with such a simple model.

In [Planck Collaboration Int. XXXIV \(2014\)](#), we analysed the polarization data in the Rosette Nebula, combining *Planck* data with rotation measures. The combination allowed to remove the degeneracy for the orientation of the magnetic field derived from rotation measures, yielding an estimate for the magnetic field intensity of 9-12 μG in the Rosette’s parent molecular cloud.

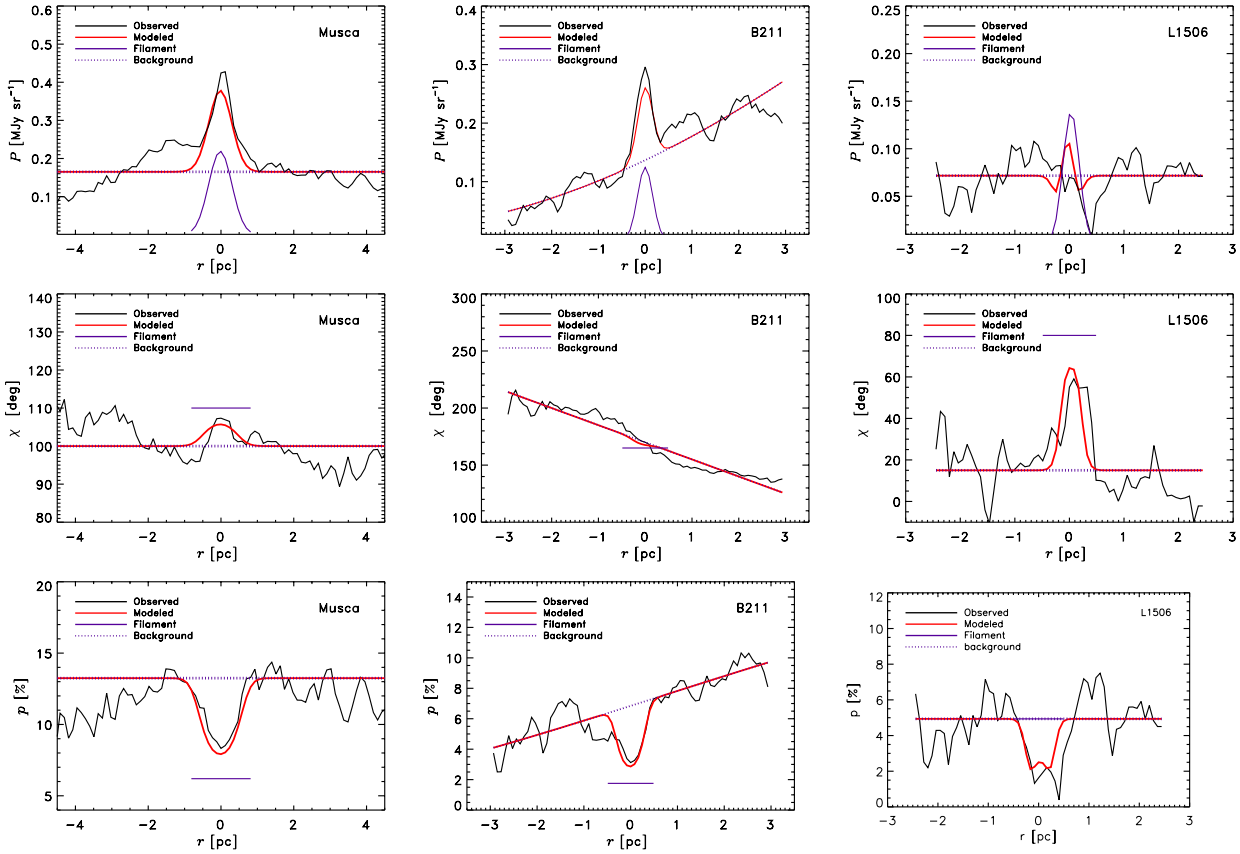


FIGURE 4.3 – Observed and modelled profiles of the polarized intensity P_{353} at 353GHz (top), the magnetic field angle χ in the plane of the sky (middle), and the polarization fraction (bottom) for the Musca filament (left column), the B211 (middle column) and L1506 (right column) filaments in Taurus. The red profiles are derived from the best-fit Q and U profiles for a maximal dust polarization fraction $p_{\max} = p_0 = 0.15$ (see Eq. 2.3). The profiles in black are the observed profiles. The profiles in purple correspond to the intrinsic polarization parameters of the filament. The dashed blue curves are derived for the background. From [Planck Collaboration Int. XXXIII \(2015\)](#).

Chapitre 5

Dust models and *Planck* results in polarization

Before *Planck*, dust models had no problems achieving the maximal polarization fraction of 3% observed in the optical (Serkowski et al. 1975; Andersson et al. 2015), as well as the 10% of polarization observed at 100 μm (Hildebrand et al. 1995), even with moderately elongated particles (*e.g.* Martin 2007; Draine & Fraisse 2009), if the larger grains were allowed to be perfectly aligned. With its maximal observed polarization fraction of 20%, *Planck* brings now challenging constraints to dust models in polarization.

Section 5.1 details the *Planck* results on the spectral properties of dust in polarization, in the submillimeter and with its relation to starlight polarization in the optical. Section 5.2 reviews the question of the maximal polarization fraction observed in extinction and in emission, and the subsequent intrinsic dust polarization fraction, as a function of the environment. Section 5.3 presents a synthetic view on the *Planck* observational constraints for dust models, in total and polarized intensity per H and per unit extinction. Section 5.4 presents some dust models derived from Compiegne et al. (2011), and compatible with all these constraints (*work in progress*).

5.1 Spectral properties of dust in polarization as seen by *Planck*

Two Planck Intermediate Results articles were focused on the spectral properties of dust in polarization (Planck Collaboration Int. XXI 2015; Planck Collaboration Int. XXII 2015).

Correlating *Planck* with starlight polarization

In the first article, which I was leading in collaboration with Peter Martin, we correlated *Planck* polarization data with starlight polarization in the optical (Heiles 2000). By correlating polarization measures between two frequencies, one can remove the common dependence of polarization data at both wavelengths : the dependence on the alignment efficiency (the Rayleigh reduction factor R_{rf}) and on the magnetic field orientation and structure (F and $\cos^2 \gamma$), which are similar (though not exactly the same) at first order in extinction and

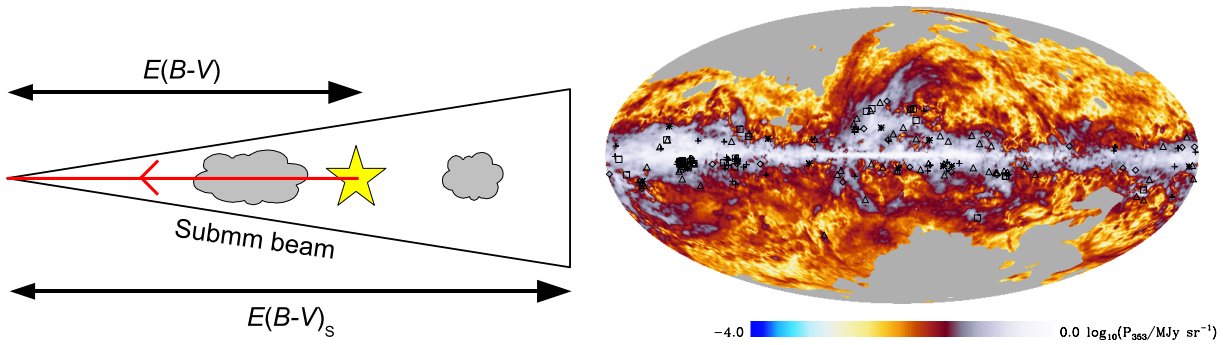


FIGURE 5.1 – (Left) Instrumental-beam and line-of-sight components affecting the comparison of polarized emission with interstellar polarization from differential extinction of a star. $E(B - V)$ is the colour excess to the star, while $E(B - V)_s$ is the submillimetre optical depth converted to a colour excess. (Right) Galactic lines of sight selected (206). The background image is of debiased polarized intensity, P_{353} , at a resolution of 1° in a Mollweide projection centred on the Galactic centre. From [Planck Collaboration Int. XXI \(2015\)](#)

in emission. The correlation coefficient then characterize what is left, *i.e.* the properties of dust grains, independently of their dynamics and orientation : their size, shape and optical properties at the two wavelengths.

Correlating P_{353}/I_{353} with p_V/τ_V is risky because both P_{353} and p_V are biased by noise (see Section 3.1). Fortunately, one can also correlate extinction and emission polarization data in Q and U . Indeed, if the same dust grains are observed at both wavelengths, polarization angles in extinction and in emission should be perpendicular. As a rotation by 90° of the polarization angle corresponds to a change in the sign of Q and U , Stokes parameters Q and U should correlate as well as P .

Before correlating data in extinction and in emission, we must check that there is no indication of a background to the star (Fig. 5.1, left). For this, the comparison of the dust optical depths at 353 GHz and in the V band turned out to be more efficient than controlling the distance to the star. To concentrate on the diffuse ISM, supposedly more simple, we also removed lines of sight with significant CO using *Planck* CO map. Low SNR data ($\text{SNR} < 3$) were also removed. This selection process considerably reduced our sample from more than 5,000 to 206 stars. Fortunately, selected stars span all latitudes and longitudes (Fig. 5.1, right). The reason for this drastic drop in the statistics is in the lack of high-SNR *extinction* (not polarization) measures in the diffuse ISM outside of the galactic plane.

The correlation between the two frequencies was found to be excellent (Fig. 5.2). This confirms that, at both wavelengths, we look at the same grains and that the dependence of the polarization with the alignment efficiency and magnetic field structure are similar. The polarization fraction in extinction p_V/τ_V and the polarization fraction in emission P_{353}/I_{353} correlate well, but the starlight polarization p_V and the polarized emission P_{353} correlate even better. These correlations provide two new ratios characteristic of the dust polarization properties in the low-latitude diffuse ISM : $R_{s/V} = (P_{353}/I_{353})/(p_V/\tau_V) = 4.1$, and $R_{P/p} = P_{353}/p_V = 5.4$ MJy/sr. Comparison with models ([Martin 2007](#); [Draine & Fraise 2009](#)) showed that models were off by $\sim 30\%$ for the first ratio, which is quite satisfactory, but by 150 % (a factor 2.5, more problematic) for the second ratio. Here, like in intensity, dust

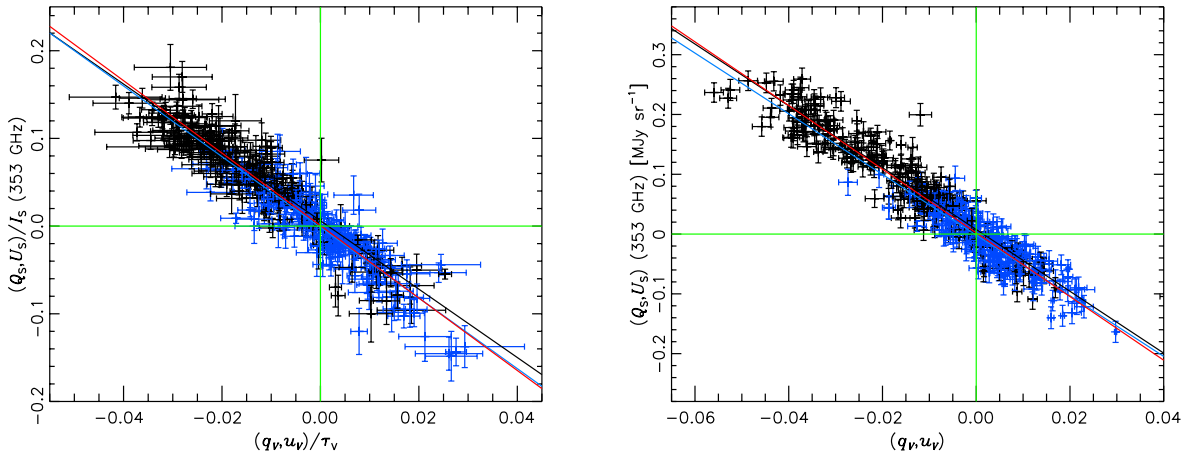


FIGURE 5.2 – (Left) Correlation of polarization fractions in emission with those in extinction for the joint fit in Q (black) and U (blue), and the joint fit in (Q,U) (red). (Right) Correlation of polarized intensity in emission (MJy/sr) with the degree of interstellar polarization. Lines for the independent fits to Q (black) and U (blue), and joint fit to (Q,U) (red) are shown. From [Planck Collaboration Int. XXI \(2015\)](#).

grains in models were found to be not emissive enough.

Submm frequency dependence

The goal of the second article was to characterize the spectral dependence of the total and polarized intensity in the diffuse ISM, providing the information necessary to clean the microwave data from the dust foreground in our search for the B-modes of the CMB. This hard work lead by T. Ghosh and F. Boulanger involved dealing with the systematics in the data, improved from one data version to another, as well as with the necessary recalibration of the FIRAS data. For the red mask of Fig. 5.3 (left), the dust spectral index β_I in total intensity I was found to be remarkably constant over the full spectral range covered by Planck and DIRBE : $\beta_I = 1.51 \pm 0.01$. With the DX11d version of the data, no flattening of the SED in the submillimeter was observed anymore, closing a pending question since WMAP observations. The polarization index, measured on a much smaller spectral range (from 353 GHz down to 70GHz for dust), is close to β_I : $\beta_P = 1.59 \pm 0.02$, assuming the same temperature for (total) dust and aligned dust. Dust looked suprisingly simple, more simple in polarization than in total intensity. This small difference in β means that P/I is almost flat, but slightly decreasing with the wavelength (Fig. 5.3, right).

5.2 Maximal dust polarization fraction in extinction and in emission

Taking raw data, to a maximal polarization fraction of 3% in extinction and of 20% in emission should correspond a polarization ratio $R_{s/V}$ of $\sim (P_{353}/I_{353})/(p_V/\tau_V) = 20/(3 \times$

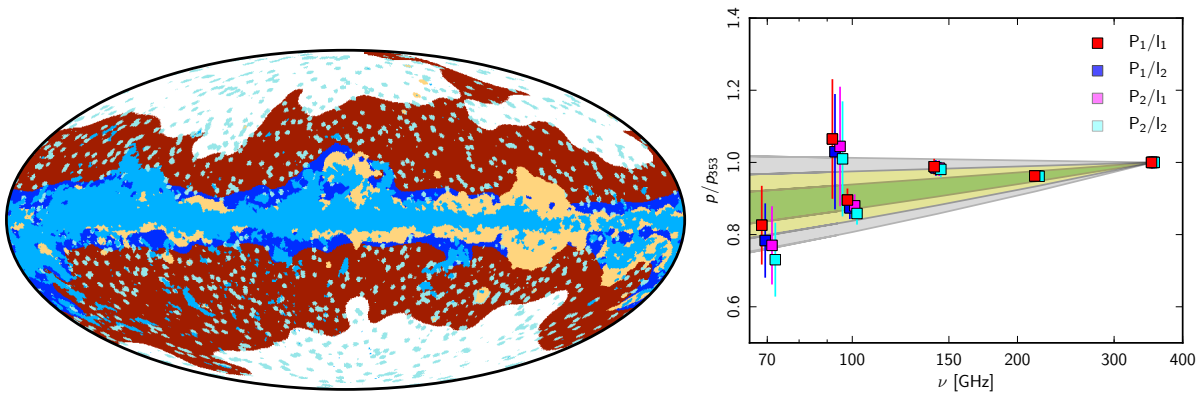


FIGURE 5.3 – (Left) Global mask used in the analysis of [Planck Collaboration Int. XXII \(2015\)](#). It comprises the CIB mask (white region), the CO mask (light-blue), the free-free mask (beige), the Galactic mask (deep-blue), and the mask of point sources (turquoise). We use the red regions of the sky. (Right) Frequency dependence of the submillimeter polarization fraction P/I in the red mask, normalized at 353 GHz. From [Planck Collaboration Int. XXII \(2015\)](#).

$1.086) \sim 6^{12}$, well above the value $R_{s/V} = 4.1$ found in [Planck Collaboration Int. XXI \(2015\)](#). Such a calculation is however incorrect for two reasons.

First, the maximal P/I of 20% has been measured recently with a huge statistics ($\sim 200,000$ pixels at a 1° resolution, see [Planck Collaboration Int. XIX 2015](#)), allowing a measure of the maximal P/I as a function of the column density. On the contrary, the 3% in extinction is based upon a few hundreds of lines of sight to stars, not very much updated since [Serkowski et al. \(1975\)](#), and with a single value derived for p_V/A_V , independent of A_V (for $0.3 < A_V < 2$). This difference in statistics, which would not be important for the derivation of the *mean* polarization fraction, is fundamental when we try to estimate the *maximal* polarization fraction. In [Planck Collaboration Int. XXI \(2015\)](#), we showed that, with a similar statistics like for starlight measures, we would have found a maximal polarization fraction in emission of 14%, compatible with the 3% in extinction and our derived value for $R_{s/V}$.

Second, the resolution of the *Planck* map of P/I is 1° , meaning that the maximal observed polarization fraction is, because of beam depolarization, *underestimated* with respect to the pencil-beam measures of starlight polarization. At the infinite resolution of starlight measures, P/I would reach at least 20-25% in the 353 GHz sky.

Regions where P/I peaks in *Planck* maps have nothing particular (Fig. 3.2). They are found everywhere in the sky, in the envelope of clouds or in diffuse regions. We have seen that P/I decreases with N_H , and how this is interpreted as a effect of the magnetic field, and not of a drop in grain alignment, in the frame of MHD simulations (Section 3.2.2). Whatever the reason for this decrease, the intrinsic dust polarization fraction, which is theoretically measured under the conditions of optimal alignment for both the dust grain and the magnetic field, should be higher than what is actually observed, at the very least 20% in diffuse regions. Dust models need therefore to be able to reproduce an *intrinsic* polarization fraction of $\sim 20 - 25\%$ to account for *Planck* observations of the polarization

12. $\tau = 1.086 A_V$

TABLE 5.1 – Planck constraints for dust models. References are, for Planck papers, XI¹, XVII², XXIX³, XIX (PIP75)⁴, XXI⁵, XXII⁶, and [Serkowski et al. \(1975\)](#); [Andersson et al. \(2015\)](#)⁷

	High-latitude DISM	Low-latitude DISM
$E(B - V)$	$E(B - V) < 0.1$	$0.15 < E(B - V) < 0.8$
I_{353}/A_V (MJy/sr)	$0.9^3 - 1.0$	1.2^5
I_{353}/N_H (MJy/sr/1e20)	0.039^1	$0.064 = 1.2/18.7$
N_H/A_V ($\times 1e20$)	$0.9^3/0.039^1 = \text{Bohlin} \times 1.23$	$\text{Bohlin} ? = 18.7$
SED from 12 μm to 100 GHz	DX9 ^{1,2,3}	DX11 (Fig. 5.4), DX9 ⁵
UV-to-NIR Extinction curve	-	Mathis (1990)
UV-to-NIR Polarization curve	-	Serkowski et al. (1975) ; Martin et al. (1992)
Polarization SED $P/I(\lambda)$	P/I slightly decreasing ⁶	flat between 353 and 217 ⁵
P_{353}/I_{353} (%)	$> 20\%^4$	$> 13.2\%^5$
p_V/A_V	-	$\sim 3\%^7$
$R_{P/p} = P_{353}/p_V$ (MJy/sr)	-	5.4^5
$R_{s/V} = (P_{353}/I_{353})/(p_V/\tau_V)$	-	4.1^5
Dust intrinsic $C_{\text{pol}}^{353}/C_{\text{ext}}^{353}$	20 – 25%	20 – 25%
Dust intrinsic $C_{\text{pol}}^V/C_{\text{ext}}^V$	4.5 – 5.6%	4.5 – 5.6%

sky.

Assuming ¹³ a polarization ratio $R_{s/V}$ of 4.1 as per [Planck Collaboration Int. XXI \(2015\)](#), a dust intrinsic polarization fraction of 20% in emission in turn corresponds to a dust intrinsic polarization fraction p_V/A_V of $\sim 4.5\%$ in the optical. This *intrinsic* value of the optical polarization fraction is significantly higher than the usual *observed* one of 3%. It is indeed not observed but, with the low statistics of starlight optical polarization, also not excluded by starlight data (see Fig. 6 of [Planck Collaboration Int. XXI 2015](#)). It is not observed just like the 20% in emission would not be significantly observed with the same low statistics.

5.3 Synthetic view on *Planck* observational constraints for dust models

Table 5.1 sums up the new constraints from *Planck* in total and polarized intensity. We need to make a distinction between two different astrophysical environments : 1) the high-latitude diffuse ISM, with its very low column densities ([Planck Collaboration XI 2014](#); [Planck Collaboration Int. XVII 2014](#); [Planck Collaboration Int. XXIX 2014](#); [Planck Collaboration Int. XXII 2015](#)) and 2) the low-latitude diffuse ISM ([Planck Collaboration Int. XXI 2015](#)), with $A_V \sim 1 - 1.5$. Dust models ([Draine & Li 2007](#); [Draine & Fraisse 2009](#);

13. The polarization ratio $R_{s/V}$ and $R_{P/p}$ do not depend, at the first order, on the dust alignment and magnetic field structure. Therefore, the *intrinsic* polarization ratios are equal to the *observed* ones, at the first order.

(Compiegne et al. 2011; Jones et al. 2013; Siebenmorgen et al. 2014) are usually calibrated on the low-latitude DISM for the extinction and polarization curve in the optical (Serkowski et al. 1975; Mathis 1990; Fitzpatrick 1999), and on the high-latitude DISM for the dust SED (DIRBE, and FIRAS before *Planck*). Such inconsistency is not new : one has always been forced to gather observables from different origins to build a set.

Still, these two environments differ in their dust properties : 1) the intensity at 353 GHz per unit extinction, I_{353}/A_V is lower by $\sim 20 - 30\%$ in the high latitude than in the low latitude ISM, 2) *Planck* Collaboration XI (2014) has shown that the ratio N_H/A_V measured with QSOs differ from the one derived toward local stars by Bohlin et al. (1978) and Rachford et al. (2009), by $\sim 20\%$, confirming Liszt (2014) ; 3) Extinction and polarization curves have never been measured in the very tenuous high latitude sky, so the polarization ratios $R_{s/v}$ and $R_{p/p}$ presented in the previous section are not yet measured in this medium.

In the following, we present different models compatible with these data for the low latitude DISM for which all observational constraints are consistent.

5.4 Toward new dust models (*work in progress*)

To satisfy *Planck* new constraints, all dust models need *very emissive* dust particles. This is already the case for the pre-*Planck* model of Jones et al. (2013), at least in total intensity, as shown in Section 1.4. Adapting it to satisfy polarization data is in progress, but is a long process due to the more elaborated structure of the grains of the Jones et al. (2013) model (core-mantles, with size-dependent optical properties). The Draine & Li (2007) model is currently being revised (Draine & Hensley 2013; Hensley & Draine 2015), with a focus on the modeling of the frequency dependence of P/I through the *magnetic dipole emission* of magnetic grains.

Here, we present a modification of the Compiegne et al. (2011) model that satisfy *Planck* constraints.

Grain shape The Compiegne et al. (2011) model is, in intensity, by 25% under the data (Section 1.4). The emissivity of silicate and carbon grains is too low compared to *Planck* observations, but this is simply an effect of the low emissivity of spheres. Elongated grains, necessary to produce polarization, will also have a greater emissivity (Siebenmorgen et al. 2014). We model silicate grains by elongated prolate or oblate spheroids. We denote a_{\parallel} the dimension of the grain along its symmetry axis, a_{\perp} its dimension perpendicular to it, and $\epsilon = a_{\parallel}/a_{\perp}$ the axis ratio. Prolate grains therefore have $\epsilon \leq 1$, while oblate grains have $\epsilon \geq 1$. We denote *elongation* the ratio of the dimensions of the larger axis to the smaller axis, which is always larger than 1. Polarization and absorption cross-sections are calculated with the T-MATRIX codes for fixed and random orientations.

Silicate optical properties The Compiegne et al. (2011) model uses the Draine & Li (2007) astrosilicates. The spectral index of the Draine & Li (2007) silicate used in Compiegne et al. (2011) is the result from a modification by Li & Draine (2001) of the traditional Draine & Lee (1984) silicates : the spectral index β was decreased from 2 to 1.6 for $800 \mu\text{m} < \lambda < 1 \text{ cm}$ in order to fit the WMAP point at 94 GHz (Li & Draine 2001). Since the DX11 version

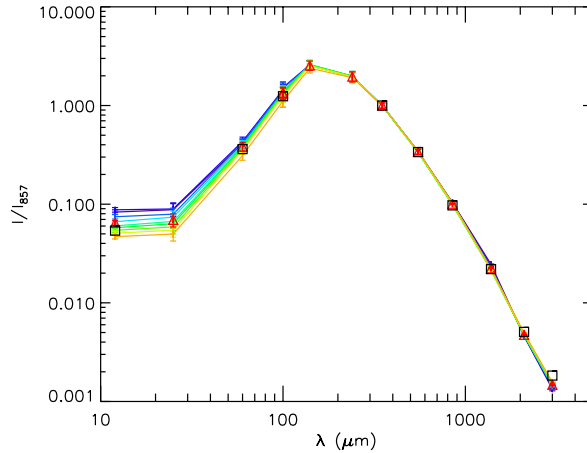


FIGURE 5.4 – Family of 9 dust SED in the ISM, binned in the value of the *Planck* intensity at 857 GHz. The mean value is plotted in red symbols. Black squares correspond to the mean SED of [Planck Collaboration Int. XXI \(2015\)](#). *Work in progress*

of *Planck* data has shown that there is no flattening anymore of I in the submillimeter, and that the dust SED is consistent with a single β from 3000 GHz down to 100 GHz, we prefer to go back to the pre-2001 silicate, the so-called smoothed astronomical silicate ([Draine & Lee 1984](#); [Laor & Draine 1993](#); [Weingartner & Draine 2001](#)) with its uniform FIR-submillimeter $\beta = 2.0$.

Dust Model We simplify the [Compiegne et al. \(2011\)](#) dust model : 1) only one population of PAH is used, the neutral one, modelled by a log-normal (width $\sigma = 0.4$, center radius a_0); 2) the VSG population is suppressed; 3) amorphous carbon grains (BE type, [Zubko et al. 1996](#); [Compiegne et al. 2011](#)) and silicate grains ([Weingartner & Draine 2001](#)) are of spheroidal shape (prolate or oblate) of the same elongation; 4) the size distributions of carbon and silicate grains are simple power-laws (with minimal and maximal sizes a_{\min} and a_{\max} , slope α).

Observations Extinction curve is that of [Mathis \(1990\)](#). Polarization curve is the so-called Serkowski’s curve, with $\lambda_{\max} = 0.55 \mu\text{m}$ and $K = 0.92$ ([Draine & Allaf-Akbari 2006](#); [Draine & Fraisse 2009](#)). The dust SED is a revised version of the mean *Planck* SED in the diffuse ISM. It is shown in Fig. 5.4, and is compatible with the mean SED observed towards the 206 stars of [Planck Collaboration Int. XXI \(2015\)](#). The polarization fraction $P(\lambda)/I(\lambda)$ is that of [Planck Collaboration Int. XXII \(2015\)](#)¹⁴. For the fitting routine, errors bars are set to 10% for all data. Displayed errors bars are true *Planck* errors bars.

14. The mean polarization ratio $R_{s/V}$ at 217 GHz was found to be equal to that at 353 GHz for the 206 stars studied in [Planck Collaboration Int. XXI \(2015\)](#) (flat trend for P/I). Lower frequencies could not be checked because of the stronger noise and contamination by the CMB.

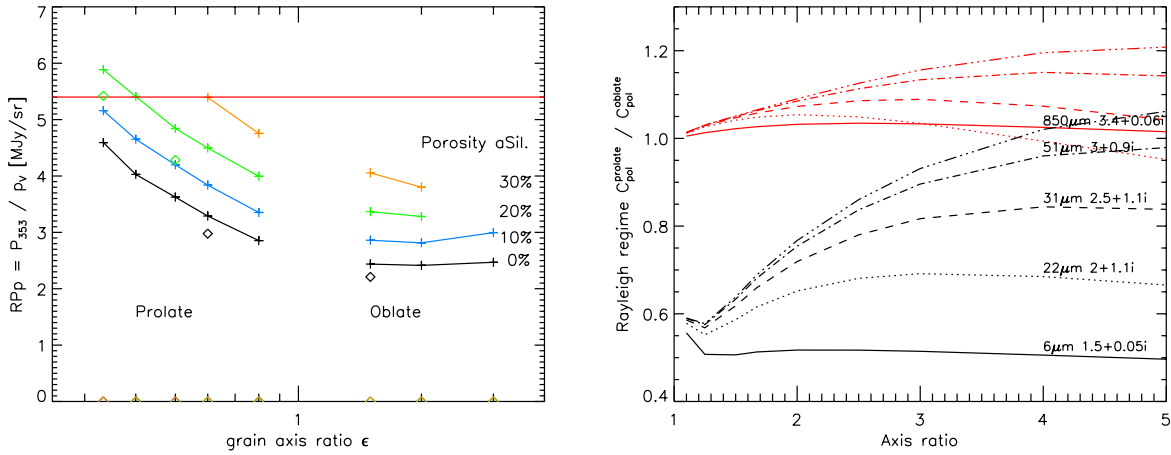


FIGURE 5.5 – (Left) $R_{P/p} = P_{353}/p_V$ as a function of the grain axis ratio $\epsilon = a_{\parallel}/a_{\perp}$. (Right) Ratio of the polarization (black) and absorption (red) cross-sections for two grains of the same elongation, the first prolate, the second oblate, obtained for the Rayleigh regime and optical index from astrosilicates, with the analytical expression presented in appendix (Chapter 7). *Work in progress.*

Parametrization of the dust alignment The alignment efficiency f is modeled as a function of grain size a through 3 parameters. It increases with grain radius a from 0 to f_{max} , with a transition at $a = a_{alg}$ characterized by a stiffness s .

$$f(a) = f_{max} \left(\frac{1}{2} + \frac{1}{2} \tanh \left(4 \frac{\log(a/a_{alg})}{s} \right) \right) \quad (5.1)$$

This expression, which mimics the radius-dependence of the efficiency of radiative torques, gives satisfactory results for all our purposes.

Fitting method The extinction, polarization in extinction, emission and polarized emission curves are fitted with equal weight using the DUSTEM wrapper (Compiegne et al. 2011) and MPFIT (Markwardt 2009).

5.4.1 Constraints on the optical properties of the aligned population

The polarization ratio $R_{P/p}$ brings a constraint on the aligned population alone, whatever the optical properties of the non-aligned population (if it exists). Li & Draine (2001) astrosilicates achieve a polarization ratio $R_{P/p} = 2.2$ MJy/sr (Draine & Fraise 2009; Planck Collaboration Int. XXI 2015). To reach $R_{P/p} = 5.4$ MJy/sr, one needs to make them much more emissive, by a factor ~ 3 . Coagulating grains (Köhler et al. 2011), making them porous by including porosity in the optical properties through the Bruggeman rule (Ysard et al. 2012), or making them elongated (Siebenmorgen et al. 2014) will increase their emissivity per unit extinction significantly.

It is possible to constrain the optical properties of the aligned population with this ratio alone. For various grain elongation and porosity, we fit the polarization curve alone, with silicates only embedded in a standard radiation field ($G_0 = 1$). Fig. 5.5 (left) shows how the $R_{P/p}$ ratio of silicates depends on the grain shape and axis ratio ϵ (black curve). $R_{P/p}$ does not depend on the grain elongation for oblate shapes, while it increases significantly with the elongation for prolate shapes. This shape effect is illustrated in Fig. 5.5 (right) : prolate grains are much efficient polarizers and emitters than oblate grains of the same elongation, *if the real part of the refractive index is high*, which is the case for silicates in the far-infrared and submillimeter.

The introduction of porosity is necessary to increase $R_{P/p}$ if we accept to eliminate very elongated shapes. In Fig. 5.5 (left), porosities of $\sim 10 - 20\%$ allow to reach the observations for prolate grains with an elongation 2.5-3, but not for oblate grains.

5.4.2 Models for the low-latitude diffuse ISM

We present two distinct dust models for the low-latitude diffuse ISM (observational constraints are presented in Table 5.1) : in the first model, only silicate grains are aligned, while in the second model both carbon and silicates grains are aligned. We do not present models for the high-latitude DISM, for which the polarization ratio $R_{P/p}$ has not yet been measured.

To achieve $P/I = 20\%$, we need to increase the maximal observed polarization fraction in the optical from $\sim 3\%$ to 4.2% (see Section 5.2).

Model with only silicate aligned

It is possible to find a model with only silicate grains aligned, achieving 19% of polarization in emission, with $R_{P/p} = P_{353}/p_V = 5.42$ MJy/sr and $I_{353}/A_V = 1.17$ MJy/sr, and a ratio of total to selective extinction $R_V = 3.25$ (Fig. 5.6). Still, we have to pay the price for it :

- Weingartner & Draine (2001) astrosilicate are almost transparent in the optical and NIR, and cannot therefore polarize light by absorption. To produce the level of polarization observed in the NIR, which deviates from the log-normal shape to follow a power-law (Martin et al. 1992), one needs to introduce very large grains of the size of the wavelength ($a \sim 1 \mu\text{m}$), which will polarize light by scattering. This was already found by Kim & Martin (1995) and can be seen in the size distributions of Draine & Fraisse (2009) too. We used a size distribution with a power-law followed by an exponential decay as in Compiegne et al. (2011). This model is not satisfactory due to the sharp cut-off in the size distribution at $2 \mu\text{m}$, imposed by the numerical limitations of the T-MATRIX codes in terms of high values of $x = 2\pi a/\lambda$.
- The total mass in silicates must be high to achieve the high polarization fraction of 20% : we need 42 ppm (not taking into account the reduction of the mass due to porosity). This increases the $9.7 \mu\text{m}$ extinction band to values which are too high with respect to the Mathis (1990) extinction curve.
- The silicates, with their spectral index $\beta = 2.0$ much higher than the observed spectral index of total intensity (~ 1.5), produce a wavelength dependence of P/I which is

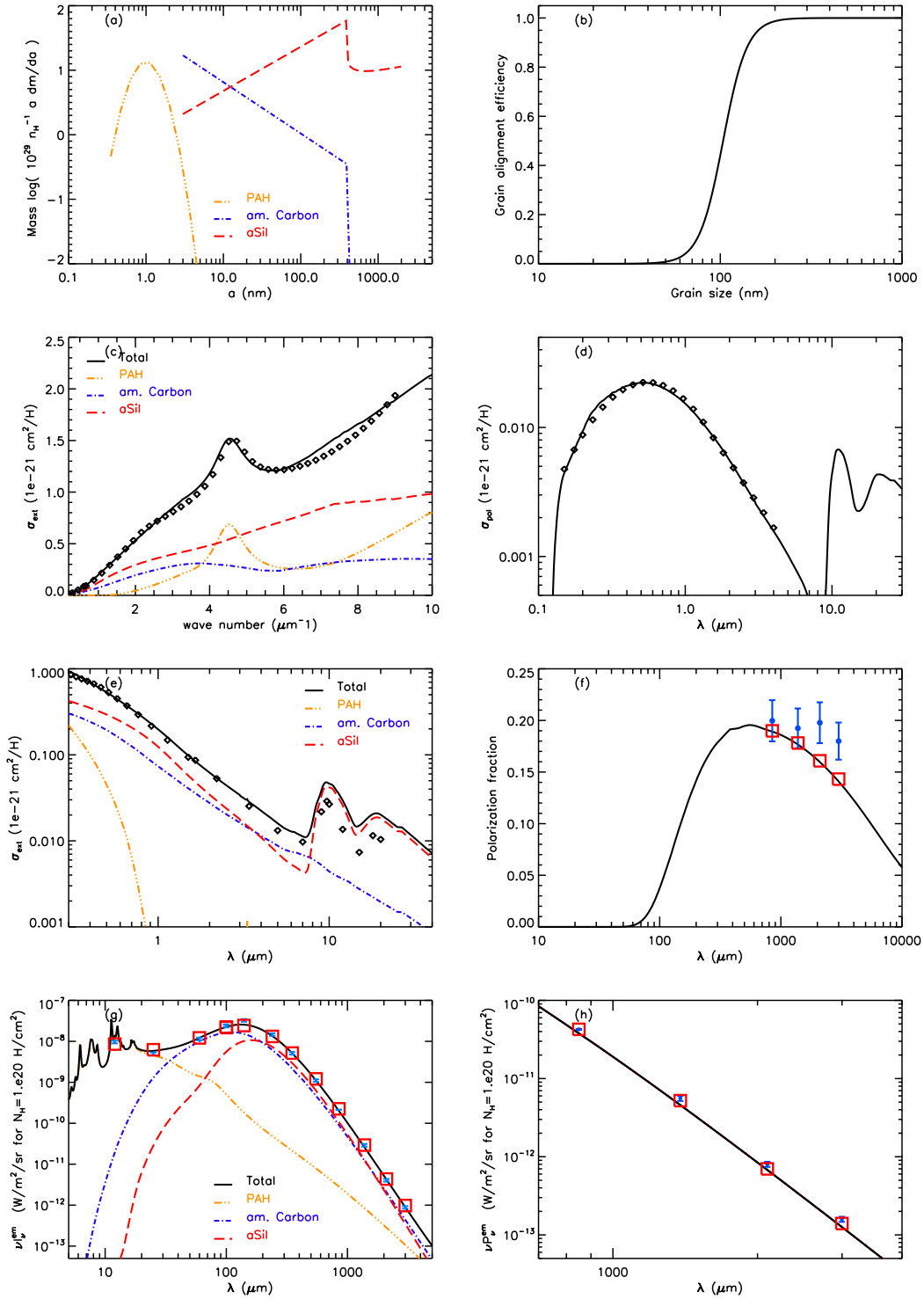


FIGURE 5.6 – Model with prolate grains of elongation 3 and with 10% of porosity. Only silicates are aligned with the magnetic field. The radiation field intensity is $G_0 = 1.1$. Red boxes are the color-corrected fluxes in the *Planck* bands. (a) Size distribution, (b) alignment function, (c) extinction curve from the UV to the optical, (d) polarization curve in extinction, (e) extinction curve from the optical to the NIR, (f) polarization fraction in emission P/I , (g) Total SED, (h) Polarized SED.

decreasing too fast.

- The polarization fraction at 100 μm is low ($\sim 3\%$). Ground observations by [Hildebrand et al. \(1995\)](#) found a polarization fraction up to 10% at 100 μm , albeit in regions which probably have a much higher radiation field than in our model here.

Model with silicate and carbon aligned

If we allow for the alignment of carbon grains, we are also able to provide a model satisfying our constraints (Fig. 5.7). The model ratios are $R_{P/p} = 5.36$ MJy/sr, $R_{s/V} = 4.12$, $I_{353}/A_V = 1.20$ MJy/sr. The ratio of total to selective extinction is $R_V = A_V/E(B-V) = 3.0$.

- With carbon grains aligned, there is no need any more for large ($> 0.5 \mu\text{m}$) grains to correctly fit the NIR polarization curve. The power-law behaviour is obtained through the differential *absorption* of carbon grains, and not through the differential *scattering* of silicate grains. This suggests an elegant explanation for the deviation of the Serkowski's curve from the log-normal shape in the NIR, and predicts a correlation between this flattening in the NIR and the decreasing trend of P/I .
- The mass of silicate required for this model is low (30 ppm). This means that a polarization fraction significantly higher than 20% is achievable, by using more silicate and aligning them better. Inversely, we can also use more silicate mass and not align them perfectly, if the alignment process does not achieve a perfect spinning alignment, and we would still achieve 20% of polarization in emission.
- The fact that in our model the fraction of polarization P/I decreases a little faster than the data comes from the rising emission of PAHs when approaching 100 GHz. This thermal contribution is however not well constrained from the observational point of view, and a lower contribution from PAHs would reconcile the model with the data.
- This model predicts a higher polarization fraction at 100 μm ($\sim 7\%$, see Fig. 5.7 (f)) than when only silicates are aligned ($\sim 3\%$, see Fig. 5.6 (f)).

Table 5.2 recapitulates our model parameters and the reduced χ^2 of the different fits. They are smaller than 1 for all our 4 observational curves, indicating that our fit is better than 10%, even better than 5% for polarization. We obtained a significantly better fit to the total SED (reduced χ^2 of 0.7 instead of 1.4) with a radiation field intensity G_0 of 1.1 instead of 1. Further increasing G_0 only slightly improved the reduced χ^2 .

How do we reproduce the decrease of $P(\lambda)/I(\lambda)$?

In our modified [Compiegne et al. \(2011\)](#) model, P/I decreases with the wavelength because carbon grains, which are less efficient polarizers than silicates (or not at all polarizing if not aligned), dominate the total intensity at large wavelengths. The thermal emission of PAHs also helps to *dilute* the polarization of large grains at low frequencies. For the [Draine & Hensley \(2013\)](#) model, P/I decreases because the ferromagnetic inclusions in silicates create a negative polarization that diminishes the flat polarization of the silicate matrix.

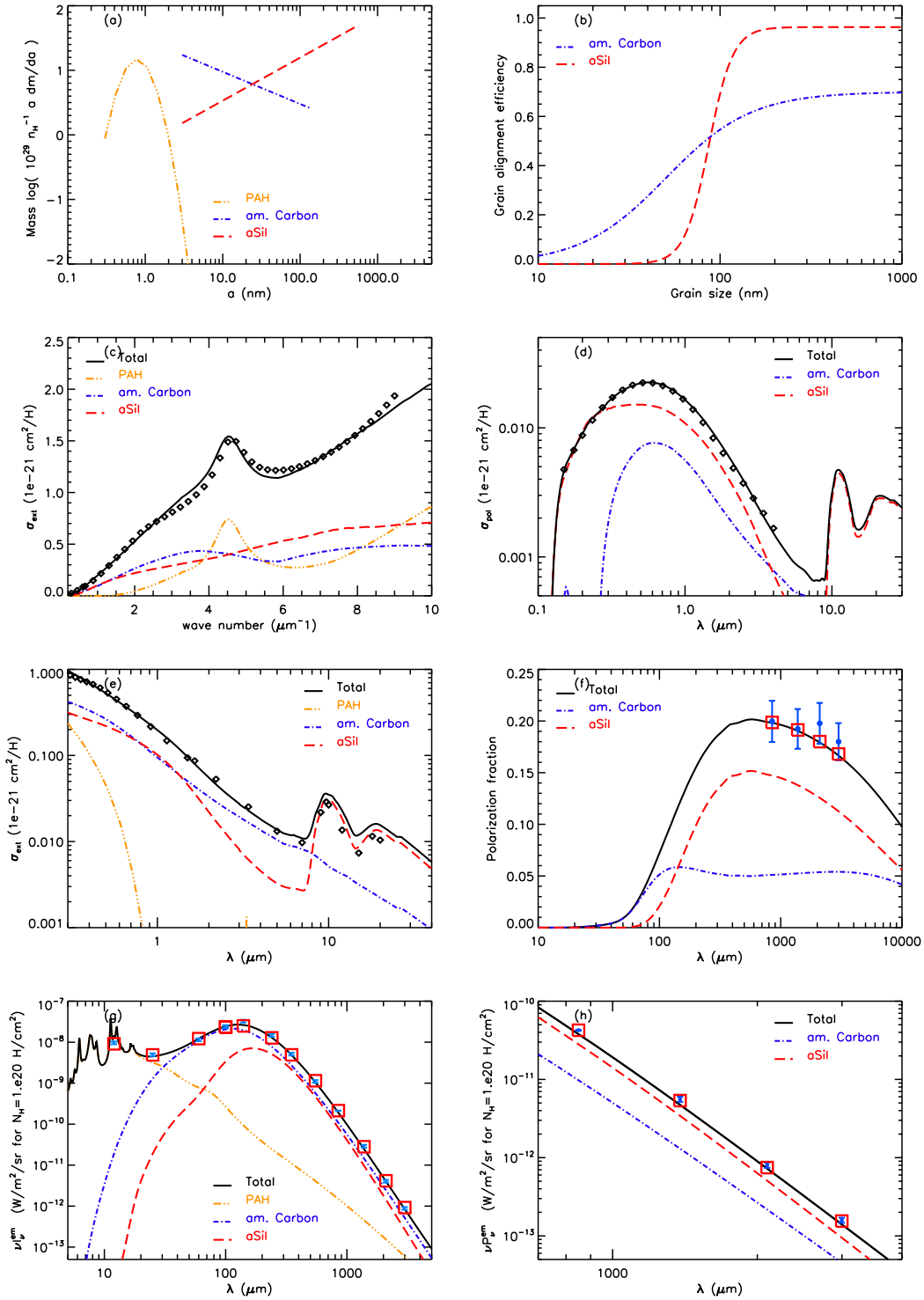


FIGURE 5.7 – Model with prolate carbon and silicates of elongation 3, both aligned with the magnetic field ($G_0 = 1.1$). Red boxes are the color-corrected fluxes in the *Planck* bands. Same legend as in Fig. 5.6.

TABLE 5.2 – Parameters for the size distribution and alignment parameters in the dust model with carbon and silicate grains aligned, for $G_0 = 1.1$. Silicate and carbon grains are prolate of elongation 3. Silicate have a 20% porosity. The reduced χ^2 are 0.70 (total intensity), 0.59 (extinction), 0.22 (polarized extinction) and 0.17 (polarized intensity). The ppm indicated ignore the porosity of the material.

Population	dust mass (per H mass)	ppm	ρ (g/cm ³)	a_0 (nm)	σ	a_{\min} (nm)	a_{\max} (nm)	α	a_{alg} (nm)	s	f_{\max}
Neutral PAH	$8.24 \cdot 10^{-4}$	69	2.24	0.48	0.4
Amorphous carbon	$1.33 \cdot 10^{-3}$	111	1.81	3	133	-4.49	50	1.87	0.70
Astrosilicate	$5.29 \cdot 10^{-3}$	30	3.0	3	542	-3.33	87	0.53	0.96

5.4.3 Conclusion

The model proposed here is a variation on the [Compiegne et al. \(2011\)](#) dust model. It uses spheroidal prolate grains, with the introduction of some porosity. We show that these small changes are sufficient to satisfy all our observational criteria, without the need for any new physics like the recent magnetic dipole emission ([Draine & Hensley 2013](#)).

We favour the model where both carbon and silicates are aligned. This model does not require a mass of silicates that would exceed cosmic abundances. It can easily achieve the 20% of polarization observed by *Planck*, and even a bit more. The carbon BE grains from [Zubko et al. \(1996\)](#) have a spectral index β which is closer to the one measured in polarization by *Planck* than silicates. The alignment of carbon grains would also give an interesting explanation to the change in the wavelength dependence of polarization in the NIR.

The model with only silicate aligned 1) does not fit so well the data, 2) requires a large mass of silicate close to the cosmic abundances, and 3) very large ($a \sim 1 \mu\text{m}$) grains. We can not exclude however that our conclusions would differ using some other kinds of silicates.

Chapitre 6

Conclusion & Perspectives

This manuscript presents a synthesis of my axis of research during the last five years within the *Planck* collaboration. It was dedicated to the study of dust emission, polarized and unpolarized, and its variations in the diffuse ISM. I have also briefly mentioned my implication in the analysis of the structure of the magnetic field. I have chosen not to focus on another important aspect of my work : the modeling and interpretation of dust evolution from the diffuse to the dense ISM (Köhler et al. 2011; Ysard et al. 2012), or in interstellar shocks in dense clouds (Guillet et al. 2007, 2009, 2011; Anderl et al. 2014). I have preferred to present the most original part of my work, possibly also the most interesting and less known by other people, that on dust polarization.

6.1 Dust evolution and polarization

Planck data has brought tight constraints on diffuse dust, and with the combination of dust extinction and dust emission, a complete set of dust-to-dust observables which models must satisfy. Dust-to-dust observables such as $R_{P/p} = P(\lambda)/p_V$ and $I(\lambda)/A_V$ have the advantage of removing the magnetic field dependence of dust polarization for the former, and removing the dust-to-gas ratio for the latter. They directly constrain the microphysics of dust, and reduce the space of model parameters.

Before *Planck* launch, we thought we would be able to determine the properties of aligned grains through the frequency dependence of polarization. We knew this would be difficult, because *Planck*, unlike PILOT, did not have high frequency channels in polarization out of the Rayleigh-Jeans regime, therefore we would not be able to measure the temperature of aligned grains. We hoped that the frequency dependence of polarization would be very different from that of total intensity, with many new complex questions. We were waiting for a new physics to define! Deceptively, dust looked rather simple in the submillimeter. Dust properties are rather uniform, and flat. This is of course very good news for the search of the B-modes of CMB polarization! Many questions that were on the wire before *Planck*, especially the variations of β with T or with λ , has now lost most of their interest, at least for the diffuse ISM where β is almost constant.

I have presented two dust models derived from Compiegne et al. (2011), rather simple and with no new physics added, compatible with *Planck* observations in total and polarized

intensities. For the moment, these model were not tested against the spectral dependence of circular polarization, or against the 3.4 and 9.7 μm bands, in absorption and in polarization. One model align silicate grains only, the other both carbon and silicates. Both models are compatible with data, meaning that *Planck* data can not answer to the question of the alignment of carbon grains. However, there a few reasons why the second model where carbon grains are also aligned is, according to me, favoured. My approach is more phenomenological than physical, but it will be helpfull to predict the amplitude of the variations of P in the diffuse ISM that contaminate the submillimeter CMB sky. The models presented here, like most dust models from the literature, use 2 populations of large grains, carbon and silicate. However, submillimeter observations of the diffuse ISM seems compatible with one single population for large grains, probably composite and possibly porous. It is in the frame of the [Jones et al. \(2013\)](#) that our team will develop such a model compatible with polarization data.

With my Phd student Lapo Fanciullo, we have just started investigating the possible correlations between dust evolution and polarization, with little success for the moment. This is a difficult subject, which combines the complexity of the grain composition with that of its shape. Calculations of cross-sections for various shapes of aggregates with DDSCAT are computer intensive. This study will also be done in the frame of a representation for the life cycle of dust as presented in [Jones et al. \(2013\)](#). Still, Lapo has demonstrated that the dust polarization ratio $R_{P/p}$ was dependent on the alignment efficiency, probably through size and temperature effects. Ironically, we tried to constrain dust evolution and we ended up bringing a new constraint on the dust alignment !

6.2 Future works (short term)

I have a few short term projects :

- The measure of $R_{P/p}$, which was in [Planck Collaboration Int. XXI \(2015\)](#) limited to low-latitude lines of sight with $0.5 < A_V < 2.5$, will be extended to the more diffuse, high-latitude, ISM using more recent starlight polarization measures ([Berdyugin et al. 2001](#); [Berdyugin & Teerikorpi 2001, 2002](#); [Berdyugin et al. 2014](#)). We will see if the evolution that is observed in I/A_V from the high-latitude to the low-latitude ISM is also observed in polarization.
- With Lapo, we will finalize the study of the variations of $R_{P/p}$ with λ_{max} , including its relation with dust evolution. We will probably need to add some other catalogs to increase the statistics. We will in the end have a complete view on the variations of $R_{P/p}$ from the most diffuse, high-latitude, sky to the interior of dense clouds.
- The models presented in Chapter 5 will be used to quantify the level of contamination of the microwave polarization by dust, in the search for the detection of the CMB B-modes.

6.3 Mid-term perspectives

My work on the structure of the magnetic field has raised my interest in the 3D inversion of the line-of-sight structure of the magnetic field. For this, starlight polarization, combined with precise measures of distance to stars (Gaia¹⁵), can be used. Together with the tracers for the gas structures (starlight extinction, DIBs), we can work toward a 3D recomposition of the magnetized ISM. This is a future project we have initiated with Rosine Lallement, with little time to work on for the moment.

With the end of the *Planck* and Herschel consortia, the focus in our research group will move from the large scales of the diffuse ISM to the small scales probed by ALMA and the JWST. We will be able to study dust evolution and polarization in accretion disks, and in the dense ISM of external galaxies. What we learned about dust from *Planck* and Herschel, together with our modeling capacities, will be useful to study the same dust physics in a different environment.

In the coming years, I plan to go abroad with my family, possibly in South America, teaching and doing my research there for a few years. This could be the moment and place for me to focus on the polarization capabilities of ALMA. During this period, I will also extend my research projects on dust in interstellar shocks with Guillaume Pineau des Forêts, Pierre Lesaffre and Sibylle Anderl.

15. Just like *Planck* was able to provide a map of CO for which it was not designed for, Gaia could be able to derive the polarization of the most bright stars, a few millions stars at all latitudes, using some asymmetry of its optics.

Chapitre 7

Appendix

Analytical expressions for the dust emission and polarization cross-sections in the Rayleigh regime

Following [Draine & Fraisse \(2009\)](#), if ζ is the angle between the oscillating electric field and the grain axis of symmetry, \vec{a} , then in the Rayleigh regime, the cross-section only depends on ζ , not on the angle between the magnetic field and the grain axis.

We note \vec{b} the unit vector in the plane of the sky, perpendicular to the grain axis of symmetry. The incident oscillating electric field can be decomposed in the reference frame of the grain

$$\vec{E} = E \cos \zeta \vec{a} + E \sin \zeta \vec{b} \quad (7.1)$$

The intensity being the square of the electric field intensity, the absorption and polarization cross-sections are, respectively

$$C_{\text{abs}} = C_{\parallel} \cos^2 \zeta + C_{\perp} \sin^2 \zeta \quad (7.2)$$

$$C_{\text{pol}} = C_{\parallel} \cos^2 \zeta - C_{\perp} \sin^2 \zeta \quad (7.3)$$

where C_{\parallel} is the cross-section for \vec{E} parallel to the grain axis, and C_{\perp} for \vec{E} perpendicular to it, in the grain frame, independently of its orientation.

The cross-sections are given for homogeneous grains (for analytical expressions for core-mantle grains, please refer to [Li et al. 2002](#)) :

$$C_{\parallel,\perp}/V = \frac{2\pi}{\lambda} \text{imag} \left(\frac{m^2 - 1}{1 + L_{\parallel,\perp} (m^2 - 1)} \right) \quad (7.4)$$

where V is the grain volume, $m = n + ik$ is the complex refractive index, $L_{\parallel,\perp}$ is the shape factor of the grain (1/3 for a sphere), e is eccentricity of the grain. a is the size of the symmetry axis of the grain, b is the size of the two other axis.

Polarization is measured in the frame (x, y) in the plane of the sky, where x is parallel to the galactic plane. z is the direction of the line of sight toward the observer. Following [Li et al. \(2002\)](#) and [Lee & Draine \(1985\)](#) :

Oblate grains ($a < b$)

$$e = \sqrt{1 - \left(\frac{a}{b}\right)^2} \quad (7.5)$$

$$L_{\parallel} = \frac{1 + e^2}{e^2} \left(1 - \frac{\arctan(e)}{e}\right) \quad (7.6)$$

$$L_{\perp} = (1 - L_{\parallel})/2 \quad (7.7)$$

$$C_{\text{pol}}^{\text{alig}} = \frac{C_{\perp} - C_{\parallel}}{2} > 0 \quad (7.8)$$

$$C_{\text{avg}} = \frac{2C_{\perp} + C_{\parallel}}{3} \quad (7.9)$$

$$C_x = C_{\perp} - C_{\text{pol}}^{\text{alig}} \sin^2 \beta \quad (7.10)$$

$$C_y = C_{\perp} - C_{\text{pol}}^{\text{alig}} (2 \cos^2 \beta \cos^2 \gamma + \sin^2 \beta \sin^2 \gamma) \quad (7.11)$$

$$(7.12)$$

Prolate grains ($a > b$)

$$e = \sqrt{\left(\frac{a}{b}\right)^2 - 1}. \quad (7.13)$$

$$L_{\parallel} = \frac{1 - e^2}{e^2} \left(\frac{1}{2e} \log \frac{1 + e}{1 - e} - 1\right) \quad (7.14)$$

$$L_{\perp} = (1 - L_{\parallel})/2 \quad (7.15)$$

$$C_{\text{pol}}^{\text{alig}} = \frac{C_{\parallel} - C_{\perp}}{4} > 0 \quad (7.16)$$

$$C_{\text{avg}} = \frac{2C_{\perp} + C_{\parallel}}{3} \quad (7.17)$$

$$C_x = C_{\perp} + C_{\text{pol}}^{\text{alig}} (1 + \cos^2 \beta) \quad (7.18)$$

$$C_y = C_{\perp} + C_{\text{pol}}^{\text{alig}} (2 \sin^2 \beta \cos^2 \gamma + \cos^2 \beta \sin^2 \gamma + \sin^2 \gamma) \quad (7.19)$$

With these definitions, we can demonstrate that the expressions for the polarization and absorption cross-sections are :

$$C_{\text{pol}} = \frac{C_x - C_y}{2} = C_{\text{pol}}^{\text{alig}} \cos^2 \gamma R_{\text{rf}} \quad (7.20)$$

$$C_{\text{abs}} = \frac{C_x + C_y}{2} = C_{\text{avg}} + R_{\text{rf}} C_{\text{pol}}^{\text{alig}} (2/3 - \cos^2 \gamma), \quad (7.21)$$

with R_{rf} the Rayleigh Reduction Factor ([Roberge & Lazarian 1999](#))

$$R_{\text{rf}} = \frac{3}{2} \left(\cos^2 \beta - \frac{1}{3} \right). \quad (7.22)$$

These last 3 expressions are valid both for prolate and oblate grains.

From the expression of the absorption/emission cross-section, we can see that the apparent dust opacity varies depending on the orientation γ of the magnetic field. Grains seem to

be more emissive when they are seen face-on (magnetic field is directed towards us, $\gamma = 90^\circ$) than when they are seen edge-on (magnetic field in the plane of the sky, $\gamma = 0^\circ$). The maximal amplitude of this variation is $R_{\text{rf}} C_{\text{pol}}^{\text{alig}}$. Converted in percentage of C_{avg} , this yields $R_{\text{rf}} C_{\text{pol}}^{\text{alig}}/C_{\text{avg}} \simeq P/I$. So C_{avg} can vary by a factor up to 20%, due to the orientation of the magnetic field.

Bibliographie

- Adamson, A. J., Whittet, D. C. B., Chrysostomou, A., et al. 1999, *The Astrophysical Journal*, 512, 224
- Anderl, S., Guillet, V., des Forêts, G. P., & Flower, D. R. 2014, arXiv.org, A69
- Anderson, C. M., Weitenbeck, A. J., Code, A. D., et al. 1996, *Astronomical Journal* v.112, 112, 2726
- Andersson, B. G. 2012, ArXiv e-prints, astro-ph.GA
- Andersson, B.-G., Lazarian, A., & Vaillancourt, J. E. 2015, *Annual Review of Astronomy and Astrophysics*, 53, 501
- Andersson, B.-G. & Potter, S. B. 2007, *The Astrophysical Journal*, 665, 369
- Arzoumanian, D., André, P., Didelon, P., et al. 2011, *Astronomy and Astrophysics*, 529, L6
- Barnett, S. J. 1915, *Physical Review*, 6, 239
- Benoît, A., Ade, P. A. R., Amblard, A., et al. 2004, *Astronomy and Astrophysics*, 424, 571
- Berdyugin, A., Piirola, V., & Teerikorpi, P. 2014, *Astronomy and Astrophysics*, 561, 24
- Berdyugin, A. & Teerikorpi, P. 2001, *Astronomy and Astrophysics*, 368, 635
- Berdyugin, A. & Teerikorpi, P. 2002, *Astronomy and Astrophysics*, 384, 1050
- Berdyugin, A., Teerikorpi, P., Haikala, L., et al. 2001, *Astronomy and Astrophysics*, 372, 276
- Bohlin, R. C., Savage, B. D., & Drake, J. F. 1978, *The Astrophysical Journal*, 224, 132
- Cardelli, J. A., Clayton, G. C., & Mathis, J. S. 1989, *The Astrophysical Journal*, 345, 245
- Cashman, L. R. & Clemens, D. P. 2014, arXiv.org
- Cayrel, R. & Schatzman, E. 1954, *Annales d'Astrophysique*, 17, 555
- Chapman, N. L., Goldsmith, P. F., Pineda, J. L., et al. 2011, *The Astrophysical Journal*, 741, 21

- Chiar, J. E., Adamson, A. J., Whittet, D. C. B., et al. 2006, *The Astrophysical Journal*, 651, 268
- Clemens, D. P., Pavel, M. D., & Cashman, L. R. 2012, *The Astrophysical Journal Supplement*, 200, 21
- Compiegne, M., Verstraete, L., Jones, A., et al. 2011, *Astronomy and Astrophysics*, 525, 103
- Das, H. K., Voshchinnikov, N. V., & Il'in, V. B. 2010, *Monthly Notices of the Royal Astronomical Society*, 404, 265
- Davis, L. & Greenstein, J. L. 1949, *Physical Review*, 75, 1605
- Davis, L. & Greenstein, J. L. 1951, *Astrophysical Journal*, 114, 206
- Del Burgo, C. & Laureijs, R. J. 2005, *Monthly Notices of the Royal Astronomical Society*, 360, 901
- Dolginov, A. Z. & Mitrofanov, I. G. 1976, *Astrophysics and Space Science*, 43, 291
- Draine, B. T. & Allaf-Akbari, K. 2006, *The Astrophysical Journal*, 652, 1318
- Draine, B. T. & Fraise, A. A. 2009, *The Astrophysical Journal*, 696, 1
- Draine, B. T. & Hensley, B. 2013, *The Astrophysical Journal*, 765, 159
- Draine, B. T. & Lazarian, A. 1998, *The Astrophysical Journal*, 508, 157
- Draine, B. T. & Lee, H. M. 1984, *The Astrophysical Journal*, 285, 89
- Draine, B. T. & Li, A. 2007, *The Astrophysical Journal*, 657, 810
- Draine, B. T. & Weingartner, J. C. 1996, *Astrophysical Journal* v.470, 470, 551
- Draine, B. T. & Weingartner, J. C. 1997, *The Astrophysical Journal*, 480, 633
- Dyck, H. M. & Beichman, C. A. 1974, *Astrophysical Journal*, 194, 57
- Fanciullo, L., Guillet, V., Aniano, G., et al. 2015, *Astronomy and Astrophysics*, 580, A136
- Fissel, L. M., Ade, P. A. R., Angilè, F. E., et al. 2015, *arXiv.org*, 5298
- Fitzpatrick, E. L. 1999, *The Publications of the Astronomical Society of the Pacific*, 111, 63
- Fitzpatrick, E. L. & Massa, D. 1988, *The Astrophysical Journal*, 328, 734
- Fitzpatrick, E. L. & Massa, D. 1990, *The Astrophysical Journal Supplement Series*, 72, 163
- Fitzpatrick, E. L. & Massa, D. 2007, *The Astrophysical Journal*, 663, 320

- Flagey, N., Noriega-Crespo, A., Boulanger, F., et al. 2009, *The Astrophysical Journal*, 701, 1450
- Franco, G. A. P. & Alves, F. O. 2015, *The Astrophysical Journal*, 807, 5
- Frisch, P. C., Andersson, B.-G., Berdyugin, A., et al. 2012, *The Astrophysical Journal*, 760, 106
- Génova-Santos, R., Martín, J. A. R., Rebolo, R., et al. 2015, *Monthly Notices of the Royal Astronomical Society*, 452, 4169
- Gerakines, P. A., Whittet, D. C. B., & Lazarian, A. 1995, *Astrophysical Journal Letters* v.455, 455, L171
- Gold, T. 1952, *Monthly Notices of the Royal Astronomical Society*, 112, 215
- Goldreich, P. & Kylafis, N. D. 1981, *Astrophysical Journal*, 243, L75
- Goodman, A. A., Jones, T. J., Lada, E. A., & Myers, P. C. 1995, *Astrophysical Journal* v.448, 448, 748
- Gorski, K. M., Wandelt, B. D., Hansen, F. K., Hivon, E., & Banday, A. J. 1999, eprint arXiv, 5275
- Guillet, V., Jones, A. P., & Pineau des Forêts, G. 2009, *Astronomy and Astrophysics*, 497, 145 (Paper II)
- Guillet, V., Pineau des Forêts, G., & Jones, A. P. 2007, *Astronomy and Astrophysics*, 476, 263 (Paper I)
- Guillet, V., Pineau des Forêts, G., & Jones, A. P. 2011, *Astronomy and Astrophysics*, 527, A123
- Hall, J. S. 1949, *Science*, 109, 166
- Hatano, H., Nishiyama, S., Kurita, M., et al. 2013, *The Astronomical Journal*, 145, 105
- Heiles, C. 2000, *The Astronomical Journal*, 119, 923
- Hensley, B. & Draine, B. T. 2015, *American Astronomical Society*, 225
- Hildebrand, R. H., Dotson, J. L., Dowell, C. D., et al. 1995, In *Astronomical Society of the Pacific*, 73, 97
- Hildebrand, R. H., Dotson, J. L., Dowell, C. D., Schlenning, D. A., & Vaillancourt, J. E. 1999, *The Astrophysical Journal*, 516, 834
- Hiltner, W. A. 1949, *Nature*, 163, 283
- Hoang, T. & Lazarian, A. 2008, *Monthly Notices of the Royal Astronomical Society*, 388, 117

- Hoang, T., Lazarian, A., & Andersson, B.-G. 2014, arXiv.org, 424
- Hoang, T., Lazarian, A., & Martin, P. G. 2013, *The Astrophysical Journal*, 779, 152
- Hong, S. S. & Greenberg, J. M. 1980, *Astronomy and Astrophysics*, 88, 194
- Houde, M., Hezareh, T., Jones, S., & Rajabi, F. 2013, *The Astrophysical Journal*, 764, 24
- Hough, J. H., Aitken, D. K., Whittet, D. C. B., Adamson, A. J., & Chrysostomou, A. 2008, *Monthly Notices of the Royal Astronomical Society*, 387, 797
- Iacobelli, M., Burkhart, B., Haverkorn, M., et al. 2014, arXiv.org, A5
- Jones, A. P., Fanciullo, L., Köhler, M., et al. 2013, *Astronomy and Astrophysics*, 558, 62
- Jones, R. V. & Spitzer, L. 1967, *Astrophysical Journal*, 147, 943
- Jones, T. J. 2003, *The Astronomical Journal*, 125, 3208
- Jones, T. J., Bagley, M., Krejny, M., Andersson, B.-G., & Bastien, P. 2015, *The Astronomical Journal*, 149, 31
- Jones, T. J., Klebe, D., & Dickey, J. M. 1992, *Astrophysical Journal*, 389, 602
- Keegstra, P. B., Smoot, G. F., Gorski, K. M., Hinshaw, G., & Tenorio, L. 1997, *Astronomical Data Analysis Software and Systems VI*, 125, 198
- Kim, S.-H. & Martin, P. G. 1995, *The Astrophysical Journal*, 444, 293
- Kogut, A., Banday, A. J., Bennett, C. L., et al. 1996, *Astrophysical Journal* v.460, 460, 1
- Köhler, M., Guillet, V., & Jones, A. 2011, *Astronomy and Astrophysics*, 528, 96
- Köhler, M., Ysard, N., & Jones, A. P. 2015, *Astronomy and Astrophysics*, 579, A15
- Laor, A. & Draine, B. T. 1993, *The Astrophysical Journal*, 402, 441
- Lazarian, A. 2007, *Journal of Quantitative Spectroscopy and Radiative Transfer*, 106, 225
- Lazarian, A. & Draine, B. T. 1997, *Astrophysical Journal* v.487, 487, 248
- Lazarian, A. & Draine, B. T. 1999, *The Astrophysical Journal*, 516, L37
- Lazarian, A. & Hoang, T. 2007, *Monthly Notices of the Royal Astronomical Society*, 378, 910
- Lee, H. M. & Draine, B. T. 1985, *Astrophysical Journal*, 290, 211
- Li, A. & Draine, B. T. 2001, *The Astrophysical Journal*, 554, 778
- Li, A. & Greenberg, J. M. 1997, *Astronomy and Astrophysics*, 323, 566

- Li, A., Greenberg, J. M., & Zhao, G. 2002, *Monthly Notices of the Royal Astronomical Society*, 334, 840
- Liszt, H. 2014, *The Astrophysical Journal*, 783, 17
- Magalhaes, A. M. 2014, XIV Latin American Regional IAU Meeting (Eds. A. Mateus, 44, 209
- Markwardt, C. B. 2009, *Astronomical Data Analysis Software and Systems XVIII ASP Conference Series*, 411, 251
- Martin, P. G. 1971, *Monthly Notices of the Royal Astronomical Society*, 153, 279
- Martin, P. G. 2007, *EAS Publications Series*, 23, 165
- Martin, P. G., Adamson, A. J., Whittet, D. C. B., et al. 1992, *The Astrophysical Journal*, 392, 691
- Martin, P. G. & Angel, J. R. P. 1976, *Astrophysical Journal*, 207, 126
- Martin, P. G., Clayton, G. C., & Wolff, M. J. 1999, *The Astrophysical Journal*, 510, 905
- Martin, P. G., Roy, A., Bontemps, S., et al. 2012, *The Astrophysical Journal*, 751, 28
- Mathewson, D. S. & Ford, V. L. 1971, *Monthly Notices of the Royal Astronomical Society*, 153, 525
- Mathis, J. S. 1986, *Astrophysical Journal*, 308, 281
- Mathis, J. S. 1990, *Annual Review of Astronomy and Astrophysics*, 28, 37
- Matsumura, M., Kameura, Y., Kawabata, K. S., et al. 2011, *Publications of the Astronomical Society of Japan*, 63, L43
- Mazzei, P. & Barbaro, G. 2008, *Monthly Notices of the Royal Astronomical Society*, 390, 706
- Misawa, R., Bernard, J. P., Ade, P., et al. 2014, in *Proceedings of the SPIE, Institut de Recherche en Astrophysique et Planétologie (France)*, 91531H
- Montier, L., Plaszczyński, S., Levrier, F., et al. 2015, *Astronomy and Astrophysics*, 574, A136
- Naghizadeh-Khouei, J. & Clarke, D. 1993, *Astronomy and Astrophysics*, 274, 968
- Pannella, M., Elbaz, D., Daddi, E., et al. 2015, *The Astrophysical Journal*, 807, 141
- Perault, M., Boulanger, F., Falgarone, E., & Puget, J. L. 1987, *Star formation in galaxies*, 2466, 97
- Planck Collaboration Int. XIX. 2015, *A&A*, 576, A104

- Planck Collaboration Int. XVII. 2014, A&A, 566, A55
- Planck Collaboration Int. XX. 2015, A&A, 576, A105
- Planck Collaboration Int. XXI. 2015, A&A, 576, A106
- Planck Collaboration Int. XXII. 2015, A&A, 576, A107
- Planck Collaboration Int. XXIX. 2014, arXiv.org
- Planck Collaboration Int. XXXII. 2014, arXiv.org
- Planck Collaboration Int. XXXIII. 2015, arXiv.org
- Planck Collaboration Int. XXXIV. 2014, arXiv.org
- Planck Collaboration Int. XXXV. 2015, arXiv.org
- Planck Collaboration XI. 2014, A&A, 571, A11
- Planck Collaboration XX. 2011, A&A, 536, A20
- Planck Collaboration XXIV. 2011, A&A, 536, A24
- Planck Collaboration XXV. 2011, A&A, 536, A25
- Plaszczynski, S., Montier, L., Levrier, F., & Tristram, M. 2013, arXiv.org, 437
- Poidevin, F., Falceta-Gonçalves, D., Kowal, G., de Gouveia Dal Pino, E., & Mário Magalhães, A. 2013, *The Astrophysical Journal*, 777, 112
- Purcell, E. M. 1979, *Astrophysical Journal*, 231, 404
- Rachford, B. L., Snow, T. P., Destree, J. D., et al. 2009, *The Astrophysical Journal Supplement*, 180, 125
- Ridderstad, M., Juvela, M., Lehtinen, K., Lemke, D., & Liljeström, T. 2006, *Astronomy and Astrophysics*, 451, 961
- Roberge, W. G. & Lazarian, A. 1999, *Monthly Notices of the Royal Astronomical Society*, 305, 615
- Roman-Duval, J., Gordon, K. D., Meixner, M., et al. 2014, *The Astrophysical Journal*, 797, 86
- Schlegel, D. J., Finkbeiner, D. P., & Davis, M. 1998, *The Astrophysical Journal*, 500, 525
- Schneider, D. P., Richards, G. T., Hall, P. B., et al. 2010, *VizieR On-line Data Catalog*, 7260, 0
- Schneider, N., Bontemps, S., Simon, R., et al. 2011, *Astronomy and Astrophysics*, 529, A1

- Serkowski, K., Mathewson, D. S., & Ford, V. L. 1975, *The Astrophysical Journal*, 196, 261
- Siebenmorgen, R., Voshchinnikov, N. V., & Bagnulo, S. 2014, *Astronomy and Astrophysics*, 561, 82
- Simmons, J. F. L. & Stewart, B. G. 1985, *Astronomy and Astrophysics* (ISSN 0004-6361), 142, 100
- Spitzer, L. & McGlynn, T. A. 1979, *Astrophysical Journal*, 231, 417
- Spitzer, L. & Tukey, J. W. 1949, *Science*, 109, 461
- Stein, W. 1966, *Astrophysical Journal*, 144, 318
- Stepnik, B., Abergel, A., Bernard, J.-P., et al. 2003, *Astronomy and Astrophysics*, 398, 551
- Trumpler, R. J. 1930, *The Publications of the Astronomical Society of the Pacific*, 42, 214
- Vaillancourt, J. E. 2002, *The Astrophysical Journal Supplement Series*, 142, 53
- Voshchinnikov, N. V. 2012, *Journal of Quantitative Spectroscopy and Radiative Transfer*, 113, 2334
- Voshchinnikov, N. V., Henning, T., Prokopjeva, M. S., & Das, H. K. 2012, *Astronomy and Astrophysics*, 541, 52
- Vrba, F. J., Coyne, G. V., & Tapia, S. 1993, *The Astronomical Journal*, 105, 1010
- Weingartner, J. C. & Draine, B. T. 2001, *The Astrophysical Journal*, 548, 296
- Weingartner, J. C. & Draine, B. T. 2003, *The Astrophysical Journal*, 589, 289
- Whittet, D. C. B. 2004, *Astrophysics of Dust*, 309, 65
- Whittet, D. C. B., Gerakines, P. A., Hough, J. H., & Shenoy, S. S. 2001, *The Astrophysical Journal*, 547, 872
- Whittet, D. C. B., Hough, J. H., Lazarian, A., & Hoang, T. 2008, *The Astrophysical Journal*, 674, 304
- Wurm, G. & Schnaiter, M. 2002, *The Astrophysical Journal*, 567, 370
- Ysard, N., Abergel, A., Ristorcelli, I., et al. 2013, *Astronomy and Astrophysics*, 559, 133
- Ysard, N., Juvela, M., Demyk, K., et al. 2012, *Astronomy and Astrophysics*, 542, 21
- Zeng, L., Bennett, C. L., Chapman, N. L., et al. 2013, *The Astrophysical Journal*, 773, 29
- Zubko, V., Mennella, V., Colangeli, L., & Bussoletti, E. 1996, *Monthly Notices of the Royal Astronomical Society*, 282, 1321